Journal of Engineering Mathematics (2005) 52: 265–291
DOI 10.1007/s10665-004-4555-2

An assessment of plasticity theories for modeling the incrementally nonlinear behavior of granular soils

CLAUDIO TAMAGNINI*, FRANCESCO CALVETTI[1] and GIOACCHINO VIGGIANI[2]

Dipartimento di Ingegneria Civile e Ambientale, Università di Perugia, Italy; [1]*Dipartimento di Ingegneria Strutturale, Politecnico di Milano, Italy;* [2]*Laboratoire 3S, UJF–INPG–CNRS, Grenoble, France;* **Author for correspondence; E-mail: tamag@unipg.it*

Received 9 August 2004; accepted in revised form 30 September 2004

Abstract. The objective of this paper is to assess the predictive capability of different classes of extended plasticity theories (bounding surface plasticity, generalized plasticity and generalized tangential plasticity) in the modeling of incremental nonlinearity, which is one of the most striking features of the mechanical behavior of granular soils, occurring as a natural consequence of the particular nature of grain interactions at the microscale. To this end, the predictions of the various constitutive models considered are compared to the results of a series of Distinct Element simulations performed *ad hoc*. In the comparison, extensive use is made of the concept of incremental strain-response envelope in order to assess the directional properties of the material response for a given initial state and stress history.

Key words: Distinct Element Method, granular materials, incremental nonlinearity, plasticity theory

1. Introduction

Nonlinearity and irreversibility are striking features of the mechanical behavior of granular soils which affect the response of virtually all geotechnical structures, such as shallow and deep foundations, excavations, tunnels, etc.

From a mathematical standpoint, the theory of plasticity has been shown to provide a convenient framework to describe these aspects of soil behavior. Early applications of perfect plasticity in geotechnical engineering, already back in the 1950s, dealt with the analysis of limit states, see *e.g.*[1,2] for a thorough account. At that time, nonlinearity and irreversibility were considered to be of importance only when dealing with failure conditions, whereas soil behavior far from failure was typically assumed as linear elastic. After the pioneering work of Roscoe and coworkers in Cambridge [3,4], the application of plasticity theories evolved towards the formulation of fully general constitutive equations for describing soil behavior in all possible initial states and loading conditions.

Over the last 20 years, a number of modifications of the classical theory have been proposed, which attempted to cover further aspects of experimentally observed soil behavior (*e.g.*, non-associativeness, intrinsic or induced anisotropy, hysteresis, soil liquefaction, strain localization into shear bands, etc.) in order to tackle other, more challenging classes of geotechnical engineering problems. These include cyclic or dynamic loading conditions (earthquakes, vibrating machines, wave loading) and soil-structure interaction in deep excavations and tunnelling, where different zones of soil experience widely different stress-paths. The breadth and depth of such scientific production is well portrayed, for example, by the proceedings of the workshops held in Grenoble [5], Cleveland [6], and Horton [7,8].

The objective of this paper is to assess the predictive capabilities of some 'extended' plasticity theories recently proposed for the analysis of cyclic behavior of soils. Rather than considering monotonic loading paths of finite and relatively large size, the main focus of this study is on the qualitative features of the *incremental* response, with particular reference to the effects of loading direction and initial state. The evaluation of the models considered is based on the comparison with a *reference* incremental response as obtained from numerical experiments with the distinct element method (DEM) on an idealized granular material consisting of a random assembly of spheres. This has been shown to be a reliable substitute for a real granular soil which allows to highlight a number of details which are very difficult, if not impossible, to extract from real laboratory experiments [9].

The structure of the paper is as follows. In Section 2, some general principles of constitutive modeling of granular materials are given and the notion of *incremental nonlinearity* is defined. The main features of the DEM model used in this study are described in Section 3, along with the details of the numerical testing program and the criteria adopted in the interpretation of the corresponding results. The details of the particular constitutive models chosen for this investigation are given in Section 4. Their predictions are then compared with the reference behavior in Section 5. Some concluding remarks are finally drawn in Section 6.

As for the notation, boldface lower- and upper-case letters are used to represent vector and tensor quantities. The symbols $\mathbf{1}$ and $\boldsymbol{I}$ are used for the second-order and fourth-order identity tensors, with components:

$$(\mathbf{1})_{ij} = \delta_{ij}, \quad (\boldsymbol{I})_{ijkl} = \frac{1}{2}(\delta_{ik}\delta_{jl} + \delta_{il}\delta_{jk}). \tag{1}$$

The symmetric and skew-symmetric parts of a second-order tensor $\boldsymbol{X}$ are denoted as: $\operatorname{sym}\boldsymbol{X} := (\boldsymbol{X} + \boldsymbol{X}^T)/2$ and $\operatorname{skw}\boldsymbol{X} := (\boldsymbol{X} - \boldsymbol{X}^T)/2$, respectively. The dot product is defined as follows: $\boldsymbol{v}\cdot\boldsymbol{w} := v_i w_i$ for any two vectors $\boldsymbol{v}$ and $\boldsymbol{w}$; $\boldsymbol{X}\cdot\boldsymbol{Y} := X_{ij}Y_{ij}$ for any two second-order tensors $\boldsymbol{X}$ and $\boldsymbol{Y}$. The dyadic product is defined as follows: $[\boldsymbol{v}\otimes\boldsymbol{w}]_{ij} := v_i w_j$ for any two vectors $\boldsymbol{v}$ and $\boldsymbol{w}$; $[\boldsymbol{X}\otimes\boldsymbol{Y}]_{ijkl} := X_{ij}Y_{kl}$ for any two second-order tensors $\boldsymbol{X}$ and $\boldsymbol{Y}$. The quantity $\|\boldsymbol{X}\| := \sqrt{\boldsymbol{X}\cdot\boldsymbol{X}}$ denotes the Euclidean norm of $\boldsymbol{X}$. The usual sign convention of soil mechanics (compression positive) is adopted throughout. In line with Terzaghi's principle of effective stress, all stresses are *effective* stresses, unless otherwise stated. In the representation of stress and strain states, use will sometimes be made of the invariant quantities p (mean stress), q (deviator stress), and θ (Lode angle), defined as

$$p := \frac{1}{3}(\boldsymbol{\sigma}\cdot\mathbf{1}), \quad q := \sqrt{\frac{3}{2}}\|\boldsymbol{s}\|, \quad \sin(3\theta) := \sqrt{6}\frac{(\boldsymbol{s}^3)\cdot\mathbf{1}}{\left[(\boldsymbol{s}^2)\cdot\mathbf{1}\right]^{3/2}} \tag{2}$$

and ϵ_v (volumetric strain), ϵ_s (deviatoric strain), $\dot{\epsilon}_v$ (volumetric strain rate), and $\dot{\epsilon}_s$ (deviatoric strain rate), defined as

$$\epsilon_v := \boldsymbol{\epsilon}\cdot\mathbf{1}, \quad \epsilon_s := \sqrt{\frac{2}{3}}\|\boldsymbol{e}\|, \quad \dot{\epsilon}_v := \dot{\boldsymbol{\epsilon}}\cdot\mathbf{1}, \quad \dot{\epsilon}_s := \sqrt{\frac{2}{3}}\|\dot{\boldsymbol{e}}\|. \tag{3}$$

In Equations (2) and (3), $\boldsymbol{s} := \boldsymbol{\sigma} - p\mathbf{1}$ is the deviatoric part of the stress tensor $\boldsymbol{e} := \boldsymbol{\epsilon} - (1/3)\epsilon_v\mathbf{1}$ and $\dot{\boldsymbol{e}} := \dot{\boldsymbol{\epsilon}} - (1/3)\dot{\epsilon}_v\mathbf{1}$ are the deviatoric parts of the strain and the strain-rate tensors, respectively, while $\boldsymbol{s}^2$ and $\boldsymbol{s}^3$ are the square and the cube of the deviatoric stress tensor, with components $(\boldsymbol{s}^2)_{ij} := s_{ik}s_{kj}$ and $(\boldsymbol{s}^3)_{ij} := s_{ik}s_{kl}s_{lj}$. It is worth noting that in $(3)_4$, with a slight abuse of notation, the symbol $\dot{\epsilon}_s$ has been employed to denote the second (deviatoric) invariant of the strain-rate tensor, which generally does not coincide with the time rate of ϵ_s, as defined in $(3)_2$.

2. Constitutive modeling of granular mterials

According to long-standing experimental evidence, the mechanical response of soils is known to strongly depend on such factors as current state, previous loading history, load increment size and direction and (possibly) time. In principle, this implies that an appropriate description of soil behavior requires the effective stress $\boldsymbol{\sigma}$ to be a function of the deformation history. Mathematically, this is expressed by the following general equation:

$$\boldsymbol{\sigma}(\boldsymbol{x},t)=\overset{\infty}{\underset{\tau=0}{\boldsymbol{\mathcal{G}}}}\left[\boldsymbol{F}^{(t)}(\boldsymbol{X},\tau)\right], \tag{4}$$

where $\boldsymbol{F}^{(t)}(\boldsymbol{X},\tau):=\boldsymbol{F}(\boldsymbol{X},t-\tau)$, with $\tau\geq 0$, is the *history* up to time t of the *deformation gradient* at a material point $\boldsymbol{X}$:

$$\boldsymbol{F}(\boldsymbol{X},t):=\frac{\partial\boldsymbol{\phi}}{\partial\boldsymbol{X}}(\boldsymbol{X},t) \tag{5}$$

associated with the motion $\boldsymbol{x}=\boldsymbol{\phi}(\boldsymbol{X},t)$ carrying point $\boldsymbol{X}$ in the reference configuration to its position $\boldsymbol{x}$ in the current configuration at time t[1]. Note that, since $\boldsymbol{\mathcal{G}}$ is a functional and not a function, the knowledge of the strain at time t is not sufficient to uniquely determine the state of stress.

As shown by [11], an inviscid material whose constitutive functional is differentiable is necessarily *elastic*. Therefore, *non-differentiable*, nonlinear functionals should be employed in the constitutive equation (4) whenever irreversible, inelastic behavior is of concern, which is the norm, rather than the exception, in geotechnical applications. However, working with nonlinear, non-differentiable functionals poses formidable mathematical problems, even in the simplest cases.

An alternative strategy, which is commonly adopted in soil modeling, is to use an incremental (or *rate-type*) formulation, in which the (objective) stress rate is given as a function of the rate of deformation $\boldsymbol{d}:=\mathrm{sym}\nabla\boldsymbol{v}$ ($\boldsymbol{v}:=\mathrm{d}\boldsymbol{\phi}/\mathrm{d}t$ being the spatial velocity) and of the current state of the material:

$$\overset{\triangledown}{\boldsymbol{\sigma}}=\mathbf{G}\left(\boldsymbol{\sigma},\boldsymbol{q},\boldsymbol{d}\right). \tag{6}$$

In (6), $\overset{\triangledown}{\boldsymbol{\sigma}}$ is the Jaumann-Zaremba stress rate, defined as

$$\overset{\triangledown}{\boldsymbol{\sigma}}:=\dot{\boldsymbol{\sigma}}+\boldsymbol{\sigma}\boldsymbol{\omega}-\boldsymbol{\omega}\boldsymbol{\sigma}, \tag{7}$$

where $\boldsymbol{\omega}:=\mathrm{skw}\nabla\boldsymbol{v}$ is the spin tensor, and $\boldsymbol{q}$ represents a set of *internal* state variables, which are introduced to account for the effects of the previous loading history. An additional set of rate equations is then required to define the evolution of the internal variables in time (*hardening laws* in the framework of classical elastoplasticity).

In the following, we will restrict ourselves to rate-independent behavior and linear kinematics. The latter assumption allows to rewrite (6) as

$$\dot{\boldsymbol{\sigma}}=\mathbf{G}\left(\boldsymbol{\sigma},\boldsymbol{q},\dot{\boldsymbol{\epsilon}}\right), \tag{8}$$

where the Jaumann stress rate $\overset{\triangledown}{\boldsymbol{\sigma}}$ has been replaced by the standard time rate $\dot{\boldsymbol{\sigma}}$, and the rate of deformation $\boldsymbol{d}$ with the (linearized) strain rate tensor $\dot{\boldsymbol{\epsilon}}$.

[1]That the state of stress at a point is solely determined by the history of the deformation gradient at that point, and does not depend on the deformation of the neighboring points, is a consequence of the principle of *local action*; see [10].

Rate-independence means that a change in the time scale does not affect the material response, *e.g.*, doubling the strain rate doubles the stress rate. More generally:

$$\boldsymbol{G}\left(\boldsymbol{\sigma}, \boldsymbol{q}, \lambda\dot{\boldsymbol{\epsilon}}\right) = \lambda \boldsymbol{G}\left(\boldsymbol{\sigma}, \boldsymbol{q}, \dot{\boldsymbol{\epsilon}}\right), \quad \forall \lambda > 0. \tag{9}$$

The above equation states that the function $\boldsymbol{G}$ is *positively homogeneous* of degree one in $\dot{\boldsymbol{\epsilon}}$. This latter property yields the following alternative expression for the constitutive equation (8):

$$\dot{\boldsymbol{\sigma}} = \boldsymbol{D}\left(\boldsymbol{\sigma}, \boldsymbol{q}, \boldsymbol{\eta}\right)\dot{\boldsymbol{\epsilon}}, \tag{10}$$

where $\boldsymbol{D}$ represents the (fourth-order) tangent stiffness tensor at the current state, which depends on the strain rate only through its *direction*, defined by the unit tensor:

$$\boldsymbol{\eta} := \frac{\dot{\boldsymbol{\epsilon}}}{\|\dot{\boldsymbol{\epsilon}}\|}. \tag{11}$$

Equation (10) provides a general representation for rate-independent constitutive equations which includes as particular cases most of the existing theories for geomaterials, including non-linear (hypo)elasticity, classical and extended plasticity, endochronic plasticity and hypoplasticity, see *e.g.* [12] and references therein. In hypoelasticity, the constitutive function $\boldsymbol{G}$ is *linear* in $\dot{\boldsymbol{\epsilon}}$, which implies that the tangent stiffness tensor $\boldsymbol{D}$ does not depend on the strain-rate direction $\boldsymbol{\eta}$. In all the other theories mentioned above, $\boldsymbol{G}$ is a *nonlinear* function of the strain rate, and $\boldsymbol{D}$ explicitly depends on $\boldsymbol{\eta}$. In this case, the material behavior is said to be *incrementally nonlinear*, see [13].

The appropriate description of the observed incrementally nonlinear behavior of granular materials is of paramount importance in constitutive modeling of granular media. This is especially relevant in a number of geotechnical engineering problems, for example in presence of cyclic loading conditions (earthquakes, vibrating machines, wave loading), or whenever different zones of soil experience widely different stress-paths, such as in deep excavations or tunnelling.

3. Incremental behavior of an analogue granular material

3.1. Preliminaries

The most natural and direct way to discriminate among the different classes of constitutive equations which are capable of describing incremental nonlinearity is to compare their predictions with the experimentally observed response of real granular materials. Conventional experiments on monotonic loading paths of finite (and quite large) size do not provide direct information in this respect. Rather, the proper definition of the incrementally nonlinear character of soil response requires the collection of data from experimental programs specifically designed in order to investigate the nature of the material response as a function of loading intensity and direction. To this end, the most natural approach is to perform a program of so-called *stress-probing* experiments, in which incremental strains are typically measured by applying a series of stress increments to a number of 'identical' specimens, with a common initial state. The stress increments (*probes*) should have an identical magnitude and point in different directions of the stress space.

As far as plasticity theory is concerned, such an experimental investigation might help answering such key questions as

(i) is there any domain of finite size in stress space where the response is incrementally linear (*i.e.*, hypoelastic)?
(ii) is the occurrence of irreversible (plastic) strains associated to some particular loading directions?
(iii) is the direction of plastic strains affected by loading direction?
(iv) is the plastic strain rate tensor coaxial to the stress tensor?

Only a few such investigations have been actually performed on sands [14,15], essentially because carrying out stress-probing experiments is, in practice, extremely difficult. First of all, in order to rule out the unavoidable differences between one specimen and another of the same soil, one might be tempted to perform all probes on a single specimen. However, this is not recommended because the application and removal of stress increments may generate irreversible deformations, thus altering the initial state of the material for subsequent probes. Therefore, as many separate specimens are needed as the number of probes, with the associated experimental difficulty of having each time a specimen which is ideally 'identical' to the others – not to speak of the time required to apply to each of them the same loading history up to the initial state. Moreover, the quality of the results crucially depends on the accuracy with which the strains are measured and the stresses are controlled, especially if the size of the probes is relatively small, as it should be to reasonably approximate the infinitesimal (tangential) response of the material. Finally, the distinction between reversible and irreversible components of the total measured strain increment requires either a constitutive assumption (typically, on the elastic behavior), or to perform for each probe a closed loading-unloading cycle.

In an attempt to circumvent these experimental problems, Bardet and Proubet [16] first suggested the use of numerical simulations with the distinct element method as a convenient tool to investigate the incremental behavior of granular materials. The numerical 'experiments' were conducted on a 2D idealized material consisting of a random assembly of circular disks. Further contributions along the same lines were later provided in the early 1990s [17–19]. This approach has been recently revived, also thanks to significant improvements of both computer power and numerical algorithms. Among the key factors, one should mention the dramatic increase of the maximum number of degrees of freedom which can be handled by modern computer architectures, a much better algorithmic description of boundary conditions, and improvements in terms of accuracy, stability and other related numerical issues. In particular, it is possible nowadays to perform fully 3D simulations in which the behavior of the idealized soil can be explored in the three-dimensional principal stress space.

An extensive program of 3D DEM simulations of stress-probing experiments was recently carried out by the authors [9,20,21]. In this paper the results of that study will serve as a reference for evaluating the performance of the elastoplastic constitutive models presented in Section 5.

3.2. Details of the DEM model

All the numerical simulations described in the following were performed with the Distinct Element code PFC-3D developed by ITASCA Consulting Group [22]. This code is the 3D generalization of the DEM code originally introduced for the analysis of rock-mechanics problems [23] and later applied to the micromechanics of analogue 2D granular materials by Cundall and Strack [24].

In PFC-3D, the soil grains are modeled as rigid spherical particles of arbitrary size, which can (slightly) overlap at the interparticle contacts. The particle interaction at the contacts is defined by appropriate contact constitutive equations, characterized by

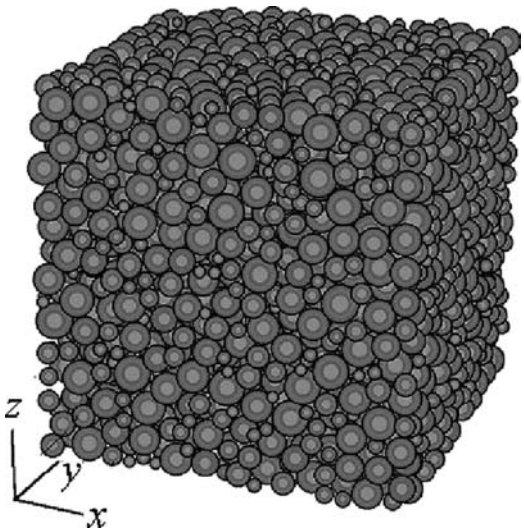

Figure 1. DEM model of a sand specimen (after [9,20,21]).

(i) linear or nonlinear (Hertzian) force-displacement law with finite normal and tangential contact stiffnesses (k_n and k_s);
(ii) intergranular slip controlled by a frictional law of Coulomb type, with friction angle ϕ_μ;
(iii) the possibility of modeling intergranular bonding at the contacts, with finite bond strength, in order to reproduce the behavior of cemented soils or soft rocks.

The equation of motion for each particle and the nonlinear contact constitutive equations at each contact are integrated in time by means of an explicit finite-difference scheme. The interested reader is referred to [25,26] for further details on the application of DEM to the modeling of idealized granular materials.

The DEM model was designed as a small but statistically equivalent sample of a real dense sand (Hostun sand), for which a limited amount of data from stress-probing experiments is available [15]. The sample is composed of about 3500 rigid and weightless spherical particles of different sizes, randomly assembled to form a cubic specimen with a side length of 4·5 mm (Figure 1). As for Hostun sand, the adopted grain-size distribution corresponds to a collection of particles with diameters ranging from 0·15 to 0·45 mm. The initial dense packing of Figure 1 is characterized by the same initial porosity (n = 0·42) of the actual sand specimens tested in the laboratory [15].

As for intergranular contacts, a linear elastic/perfectly-plastic behavior with purely frictional limit condition (no interparticle bonding) was assumed. The boundaries of the cubic specimen are defined by introducing smooth 'wall' elements, to which either stresses (through wall-applied forces) or displacement rates (through prescribed wall speed) can be imposed (walls are not shown in Figure 1).

It is important to emphasize that, contrary to most DEM studies of granular assemblies, in the interpretation of the numerical results the specimen was considered as a 'single element' subject to homogeneous states of stress and strain. No attention was paid to the details of the contact-forces distributions and local grain kinematics, the objective of the experiments being to investigate the material response from a purely phenomenological standpoint. In this respect, it can be noted that, since the walls containing the cubic specimen are frictionless, the principal directions of stresses and strains coincide with the coordinate axes x, y and z shown in Figure 1. Principal strains are

Table 1. Material parameters of the DEM model (after [9,20,21]).

k_n (kN/m)	k_s (kN/m)	$\tan(\phi_\mu)$ (–)
100·0	25·0	0·35

calculated directly from wall displacements, while the corresponding principal stresses are obtained from boundary forces, as in conventional laboratory testing.

Another fundamental issue concerns the possibility of decomposing the total computed strain increments into a reversible ('elastic') part and an irreversible ('plastic') part:

$$\Delta\boldsymbol{\epsilon} = \Delta\boldsymbol{\epsilon}^{\mathrm{e}} + \Delta\boldsymbol{\epsilon}^{\mathrm{p}}. \tag{12}$$

In earlier investigations with 2D models [17,18], a strategy based on the use of closed stress loops was adopted to compute the irreversible part of the strain increment. As for real laboratory tests, this procedure relies on the assumption that the strains occurring during unloading are purely reversible, which is, however, not always the case. A different approach was adopted in [9,20,21], where the reversible component of the strain increment was directly determined by means of an 'elastic' counterpart of the DEM specimen, in which the mechanisms responsible for energy dissipation (interparticle sliding) and structure rearrangement (opening of contacts) are inhibited at the microscale. Plastic strain increments are then computed from the kinematic decomposition (12).

The complete definition of the numerical model required the calibration of normal and shear contact stiffness, k_{n} and k_{s}, and interparticle friction angle, ϕ_μ. These parameters were determined by trial and error in order to provide a reasonable fit with the experimental data reported in [15]. In order to compensate the effect of the spherical shape of the particles in the numerical model – which could otherwise lead to unrealistically low mobilized stress ratios at ultimate failure; see [9] – all the DEM simulations were performed by keeping the particle rotations fixed. Note that the assumed boundary conditions (perfectly rigid and smooth walls) and this additional kinematic constraint tend to inhibit any inhomogeneity in the equivalent macroscopic strain field, *i.e.*, strain localization. The complete set of parameters for the DEM model is given in Table 1.

As has been thoroughly discussed by Calvetti *et al.* [9,20,21], the DEM model proves remarkably effective in describing such a complex behavior as that of a real dense sand, over a large spectrum of loading paths, both from a qualitative and – to a somewhat lesser extent – quantitative point of view. This is even more remarkable if one considers the relative simplicity of the numerical model at the microscopic level (spherical grains, simple elastic-frictional interactions at grain contacts, and fixed rotations) and the extremely low number (only 3) of material parameters required for its complete definition.

3.3. Program of numerical stress probing

As detailed in [20,21], the program of numerical stress-probing tests included the two following types of incremental loading conditions:

(a) axisymmetric probes ($\Delta\sigma_x = \Delta\sigma_y$);
(b) deviatoric probes ($\Delta\sigma_x + \Delta\sigma_y + \Delta\sigma_z = 0$).

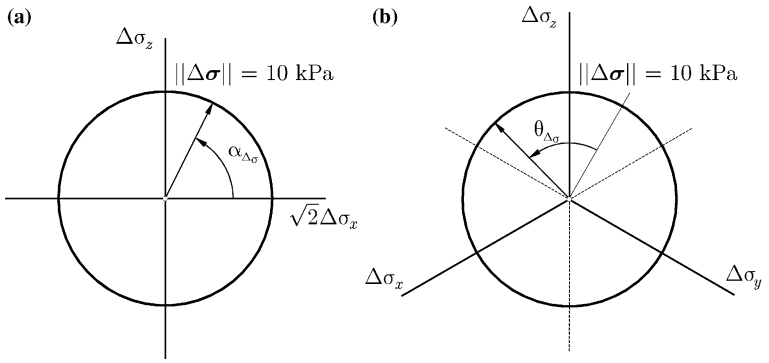

Figure 2. Incremental stress probes: (a) axisymmetric probes; (b) deviatoric probes.

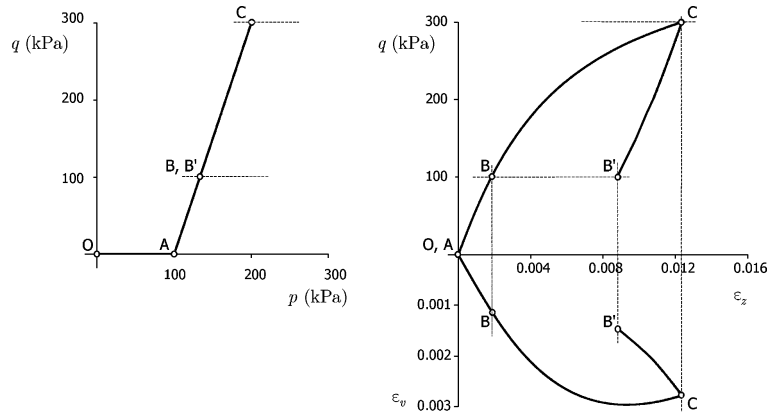

Figure 3. Stress-strain response of the DEM model upon the loading path OABCB′.

The norm of all stress probes is constant and equal to 10 kPa. The stress-probe direction is defined by the angle $\alpha_{\Delta\sigma}$ in the so-called Rendulic plane of stress increments σ_z:$\sqrt{2}\Delta\sigma_x$ for probes of type (a), and by the Lode angle of the stress increment, $\theta_{\Delta\sigma}$, for probes of type (b), see Figure 2.

In [9,20,21] several different initial states were investigated. Herein, only two of them will be considered, both characterized by the following stress state:

$$\sigma_{x0} = \sigma_{y0} = 100{\cdot}0 \text{ kPa}, \quad \sigma_{z0} = 200{\cdot}0 \text{ kPa} \tag{13}$$

but possessing a different loading history, as sketched in Figure 3. Virgin state B was reached by the two-stage stress path OA-AB, corresponding to isotropic compression and standard compression at constant confining stress, respectively. Preloaded state B′ was obtained by first loading along the path OA-AC, and then unloading along CB′.

The overall behavior of the DEM model along the loading-unloading path ABCB′ is also shown in Figure 3, in terms of deviator stress, q, and volume strain, ϵ_v, plotted as functions of axial strain, ϵ_z. Note that the net volume strain increment occurring in the closed loop BCB′ is almost negligible, *i.e.*, the porosity at B′ (n = 0·4178) is practically unchanged as compared to state B (n = 0·4176). Therefore, the two states considered differ from each other only in terms of the previous loading history.

In the following, the response of the granular assembly to the stress-probing program, as well as the predictions of the different models introduced in Section 4, is depicted by using

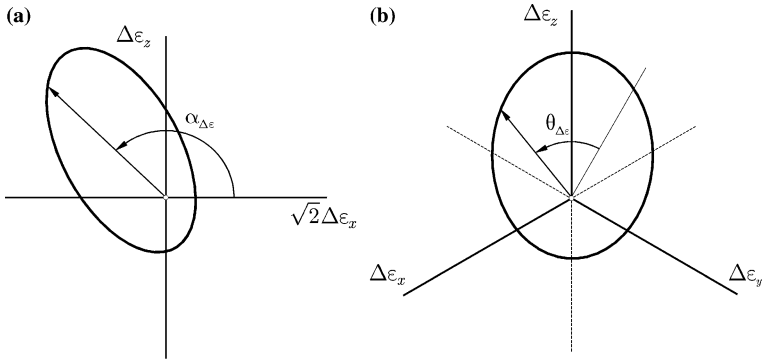

Figure 4. Incremental strain response envelopes: (a) axisymmetric probes; (b) deviatoric probes.

the so-called *incremental strain-response envelope*, as defined in [27]. Such a representation follows directly from the concept of stress-response envelope, first proposed by Gudehus [28] as a convenient tool for visualizing the properties of rate-type constitutive equations. According to Gudehus, a stress(strain)-response envelope is defined as the image in the stress(strain)-rate space of the unit sphere in the strain(stress) rate space, under the map defined by the constitutive equation. By simply replacing rates with finite-size increments, the same definitions apply to the incremental response envelopes. In the general case, an incremental strain-response envelope (RE, hereafter) is a 'surface' in a six-dimensional space. However, in the two particular loading conditions considered, the most natural choice is to represent the section of the REs in the planes of work-conjugated strain increment quantities; see Figure 4.

The size of each strain-increment vector defining the RE can be directly interpreted as a directional secant compliance of the material, for the associated loading direction and stress-increment magnitude. For a vanishing stress-increment norm, the RE asymptotically meets the strain-response envelope defined in terms of rates. Therefore, provided that the stress probes are 'small' enough, the REs obtained from numerical simulations yield useful information on the underlying constitutive behavior of the material. For example, in axisymmetric conditions, it is easy to show that an incrementally linear behavior transforms the unit circle in Figure 2a into an ellipse centered at the origin of the strain-increment plane. Thus, any significant deviation from this kind of response, such as a shift of the center of the RE from the origin or a marked asymmetry of its shape, strongly suggests some form of incremental nonlinearity.

4. Continuum plasticity models

All the models considered here have been developed as extensions of an elastoplastic constitutive model which derives from the isotropic hardening model of Nova [29] and its anisotropic hardening extension proposed by di Prisco [30,31]. The structure of the basic model is detailed in Section 4.1, while three hierarchical extensions of the formulation are presented in Sections 4.2–4.4.

4.1. Anisotropic hardening elastoplastic model

4.1.1. *General formulation*

Following the previous works of Nova and coworkers on granular soils [29–32], a constitutive model has been developed within the framework of the classical theory of anisotropic hardening elastoplasticity, which is capable to reproduce the salient features of the mechanical

response of coarse and fine-grained soils, such as pressure dependence, dilatancy, brittle-ductile transition and critical state.

As usual under the hypothesis of linear kinematics, the strain rate is decomposed additively in an elastic, reversible part, $\dot{\boldsymbol{\epsilon}}^{\mathrm{e}}$, and a plastic, irreversible part, $\dot{\boldsymbol{\epsilon}}^{\mathrm{p}}$:

$$\dot{\boldsymbol{\epsilon}} = \dot{\boldsymbol{\epsilon}}^{\mathrm{e}} + \dot{\boldsymbol{\epsilon}}^{\mathrm{p}}. \tag{14}$$

As in [33], the elastic behavior of the material is defined by postulating the existence of a strain-energy function $\psi(\boldsymbol{\epsilon}^{\mathrm{e}})$ such that

$$\boldsymbol{\sigma}(\boldsymbol{\epsilon}^{\mathrm{e}}) = \frac{\partial \psi}{\partial \boldsymbol{\epsilon}^{\mathrm{e}}}\left(\boldsymbol{\epsilon}^{\mathrm{e}}\right) \tag{15}$$

By differentiation, the hyperelastic constitutive equation in rate form is obtained:

$$\dot{\boldsymbol{\sigma}} = \boldsymbol{D}^{\mathrm{e}}\left(\boldsymbol{\epsilon}^{\mathrm{e}}\right)\left[\dot{\boldsymbol{\epsilon}} - \dot{\boldsymbol{\epsilon}}^{\mathrm{p}}\right] \tag{16}$$

in which:

$$\boldsymbol{D}^{\mathrm{e}} := \frac{\partial^2 \psi}{\partial \epsilon^{\mathrm{e}} \otimes \partial \epsilon^{\mathrm{e}}} \tag{17}$$

is the fourth-order elastic stiffness tensor.

Irreversibility is introduced by requiring the state of the material, defined in terms of the stress tensor $\boldsymbol{\sigma}$ and the internal variables $\boldsymbol{q}$, to lie in the convex set:

$$\mathbb{E}_{\sigma} := \left\{ \left(\boldsymbol{\sigma}, \boldsymbol{q}\right) \;\middle|\; f\left(\boldsymbol{\sigma}, \boldsymbol{q}\right) \leq 0 \right\}, \tag{18}$$

where $f(\boldsymbol{\sigma}, \boldsymbol{q})$ is the yield function. The evolution of plastic strains is defined by prescribing the following classical flow rule:

$$\dot{\boldsymbol{\epsilon}}^{\mathrm{p}} = \dot{\lambda}\, \boldsymbol{n}_g(\boldsymbol{\sigma}, \boldsymbol{q}), \quad \boldsymbol{n}_g := \frac{1}{g^*}\frac{\partial g}{\partial \boldsymbol{\sigma}}, \quad g^* := \left\| \frac{\partial g}{\partial \boldsymbol{\sigma}} \right\| \tag{19}$$

in which $\boldsymbol{n}_g$ defines the plastic flow direction as the normalized gradient of a scalar plastic potential $g(\boldsymbol{\sigma}, \boldsymbol{q})$ and $\dot{\lambda} \geq 0$ is the plastic multiplier.

The evolution of the internal variables is provided by the following hardening law:

$$\dot{\boldsymbol{q}} = \dot{\lambda} \boldsymbol{h}(\boldsymbol{\sigma}, \boldsymbol{q}), \tag{20}$$

where $\boldsymbol{h}$ is a suitable hardening function.

The plastic multiplier appearing in $(19)_1$ and (20) is subject to the so-called *Kuhn-Tucker complementarity conditions*:

$$\dot{\lambda} \geq 0, \quad f(\boldsymbol{\sigma}, \boldsymbol{q}) \leq 0, \quad \dot{\lambda} f(\boldsymbol{\sigma}, \boldsymbol{q}) = 0, \tag{21}$$

stating that plastic deformations may occur only for states on the yield surface. Prager's *consistency condition* requires that, for plastic loading processes ($\dot{\lambda} > 0$):

$$\dot{f} = \frac{\partial f}{\partial \boldsymbol{\sigma}} \cdot \dot{\boldsymbol{\sigma}} + \frac{\partial f}{\partial \boldsymbol{q}} \cdot \dot{\boldsymbol{q}} = 0. \tag{22}$$

When the normalized *loading direction* $\boldsymbol{n}_f$ is defined as

$$\boldsymbol{n}_f := \frac{1}{f^*}\frac{\partial f}{\partial \boldsymbol{\sigma}}, \quad f^* := \left\| \frac{\partial f}{\partial \boldsymbol{\sigma}} \right\| \tag{23}$$

and the constitutive equation (16) and the hardening law (20) are taken into account, whenever plastic loading occurs, then

$$f^* \boldsymbol{n}_f \cdot \boldsymbol{D}^{\mathrm{e}} \dot{\boldsymbol{\epsilon}} - \dot{\lambda} \left(f^* \boldsymbol{n}_f \cdot \boldsymbol{D}^{\mathrm{e}} \boldsymbol{n}_g - \frac{\partial f}{\partial \boldsymbol{q}} \cdot \boldsymbol{h} \right) = 0. \tag{24}$$

When, for all admissible states $\left(\boldsymbol{\sigma}, \boldsymbol{q}\right)$, the yield condition, the flow rule and the hardening law are assumed such that the inequality:

$$K_p := \boldsymbol{n}_f \cdot \boldsymbol{D}^{e} \boldsymbol{n}_g + H_p > 0, \quad H_p := -\frac{1}{f^*} \frac{\partial f}{\partial \boldsymbol{q}} \cdot \boldsymbol{h} \tag{25}$$

is *always* satisfied,[2] then Equation (24) provides the following expression for the plastic multiplier:

$$\dot{\lambda} = \frac{1}{K_p} \left\langle \boldsymbol{n}_f \cdot \boldsymbol{D}^{\mathrm{e}} \dot{\boldsymbol{\epsilon}} \right\rangle \tag{26}$$

in which $\langle x \rangle := (x + |x|)/2$ is the ramp function. The scalar quantity H_p in (25) is the so-called plastic modulus.

When the above expression for the plastic multiplier is substituted in (19) and (20), the time rates of $\boldsymbol{\sigma}$ and $\boldsymbol{q}$ can be expressed as functions of the corresponding rates of the total strain ϵ:

$$\dot{\boldsymbol{\sigma}} = \boldsymbol{D} \left(\boldsymbol{\sigma}, \boldsymbol{q}, \boldsymbol{\eta} \right) \dot{\boldsymbol{\epsilon}}, \quad \dot{\boldsymbol{q}} = \boldsymbol{H} \left(\boldsymbol{\sigma}, \boldsymbol{q}, \boldsymbol{\eta} \right) \dot{\boldsymbol{\epsilon}} \tag{27}$$

with

$$\boldsymbol{D} := \boldsymbol{D}^{\mathrm{e}} - \frac{\mathcal{H}(\dot{\lambda})}{K_p} \left(\boldsymbol{D}^{\mathrm{e}} \boldsymbol{n}_g \right) \otimes \left(\boldsymbol{n}_f \boldsymbol{D}^{\mathrm{e}} \right), \tag{28}$$

$$\boldsymbol{H} := \frac{\mathcal{H}(\dot{\lambda})}{K_p} \boldsymbol{h} \otimes \left(n_f \boldsymbol{D}^{\mathrm{e}} \right) \tag{29}$$

in which $\mathcal{H}(x)$ is the Heaviside step function, which is equal to 1 if $x > 0$ and 0 otherwise. Note that the dependence of $\boldsymbol{D}$ and $\boldsymbol{H}$ on the strain-rate direction $\boldsymbol{\eta}$ is controlled by the sign of the plastic multiplier; see (26).

4.1.2. *Hyperelastic behavior*

The adopted stored-energy function is the same that used in [33,36]. The function $\psi(\boldsymbol{\epsilon}^{\mathrm{e}})$ is given by the following two-invariant expression:

$$\psi(\boldsymbol{\epsilon}^{\mathrm{e}}) = \bar{\psi}(\epsilon_v^{\mathrm{e}}, \epsilon_s^{\mathrm{e}}) = \tilde{\psi}(\epsilon_v) + \frac{3}{2} \left[G_0 + \frac{\alpha}{\hat{\kappa}} \tilde{\psi}(\epsilon_v) \right] \left(\epsilon_s^{\mathrm{e}} \right)^2, \tag{30}$$

where

$$\tilde{\psi}(\epsilon_{\mathrm{v}}) := \begin{cases} \hat{\kappa}\, p_r \exp\left(\epsilon_v^e / \hat{\kappa} - 1 \right) & (\epsilon_v^e \geq \hat{\kappa}), \\ p_r \epsilon_v^e + p_r \left(\epsilon_v^e - \hat{\kappa} \right)^2 / (2\hat{\kappa}) & (\epsilon_v^e < \hat{\kappa}). \end{cases} \tag{31}$$

[2]In the general case of non-associative hardening plasticity, assumption (25) places a restriction on the amount of allowable softening, as discussed in [34] in the context of a simple one-dimensional case, excluding the possibility of *subcritical softening*, as defined in [35]. In practice, this restriction does not represent a true limitation of the theory, as this phenomenon is not observed in most geomaterials, except perhaps in very stiff, brittle rocks.

In Equations (30), (31), p_r represents a reference mean stress, while $\hat{\kappa}$, G_0 and α are material constants. From (16) and (30) the following expression for the elastic stiffness tensor is obtained:

$$\boldsymbol{D}^{\mathrm{e}} := \left[1 + \frac{3\alpha}{2\hat{\kappa}}\left(\epsilon_s^{\mathrm{e}}\right)^2\right] K_\epsilon \mathbf{1}\otimes\mathbf{1} + 2\left(G_0 + \frac{\alpha}{\hat{\kappa}}\,\tilde{\psi}\right)\left[\boldsymbol{I} - \frac{1}{3}\mathbf{1}\otimes\mathbf{1}\right] + \\ + 2\left(\frac{\alpha}{\hat{\kappa}}\right)\theta_\epsilon\left(\mathbf{1}\otimes\boldsymbol{e}^{\mathrm{e}} + \boldsymbol{e}^{\mathrm{e}}\otimes\mathbf{1}\right), \tag{32}$$

where $\boldsymbol{e}^{\mathrm{e}} := \boldsymbol{\epsilon}^{\mathrm{e}} - (\epsilon_v^{\mathrm{e}}/3)\mathbf{1}$ is the deviatoric elastic strain, and the two functions $\theta_\epsilon(\epsilon_v^{\mathrm{e}})$ and $K_\epsilon(\epsilon_v^{\mathrm{e}})$ are given by

$$\theta_\epsilon := \frac{\mathrm{d}\tilde{\psi}}{\mathrm{d}\epsilon_v^{\mathrm{e}}} = \begin{cases} p_r \exp\left(\epsilon_v^{\mathrm{e}}/\hat{\kappa} - 1\right) & (\epsilon_v^{\mathrm{e}} \geq \hat{\kappa}), \\ p_r\left(\epsilon_v^{\mathrm{e}}/\hat{\kappa}\right) & (\epsilon_v^{\mathrm{e}} < \hat{\kappa}), \end{cases} \tag{33}$$

and

$$K_\epsilon := \frac{\mathrm{d}\theta_\epsilon}{\mathrm{d}\epsilon_v^{\mathrm{e}}} = \begin{cases} (p_r/\hat{\kappa}) \exp\left(\epsilon_v^{\mathrm{e}}/\hat{\kappa} - 1\right) & (\epsilon_v^{\mathrm{e}} \geq \hat{\kappa}), \\ p_r/\hat{\kappa} & (\epsilon_v^{\mathrm{e}} < \hat{\kappa}). \end{cases} \tag{34}$$

In the range $\epsilon_v^{\mathrm{e}} \geq \hat{\kappa}$, the adopted stored-energy function describes a fully nonlinear, pressure-dependent hyperelastic behavior. It is worth noting that the adopted hyperelastic model exhibits volumetric-deviatoric coupling, which is associated with the last term on the RHS of (32). This coupling effect disappears when the state of the material is isotropic ($\mathbf{e}^{\mathrm{e}} = \mathbf{0}$), or if $\alpha = 0$.

4.1.3. *Yield function and plastic potential*

The yield function and plastic potential are given by a suitably modified version of the equations proposed by Lagioia *et al.* [33,37] to account for rotational anisotropy:

$$f(\boldsymbol{\sigma}, p_{\mathrm{s}}, \boldsymbol{\delta}^a) = f(p^a, q^a, \theta^a, p_s) \\ = \left(A_f^a\right)^{K_{1f}/C_f}\left(B_f^a\right)^{-K_{2f}/C_f} p^a - p_s = 0, \tag{35}$$

$$g(\boldsymbol{\sigma}, \boldsymbol{\delta}^a) = g(p^a, q^a, \theta^a) \\ = \left(A_g^a\right)^{K_{1g}/C_g}\left(B_g^a\right)^{-K_{2g}/C_g} p^a - \tilde{p}_s = 0, \tag{36}$$

where

$$A_\alpha^a := 1 + \frac{1}{K_{1\alpha} M_\alpha(\theta^a, \boldsymbol{\delta}^a)}\,\frac{q^a}{p^a}, \tag{37}$$

$$B_\alpha^a := 1 + \frac{1}{K_{2\alpha} M_\alpha(\theta^a, \boldsymbol{\delta}^a)}\,\frac{q^a}{p^a}, \tag{38}$$

$$K_{1\alpha} := \frac{m_\alpha(1-a_\alpha)}{2(1-m_\alpha)}\left\{1 + \sqrt{1 - \frac{4a_\alpha(1-m_\alpha)}{m_\alpha(1-a_\alpha)^2}}\right\}, \tag{39}$$

$$K_{2\alpha} := \frac{m_\alpha(1-a_\alpha)}{2(1-m_\alpha)}\left\{1 - \sqrt{1 - \frac{4a_\alpha(1-m_\alpha)}{m_\alpha(1-a_\alpha)^2}}\right\}, \tag{40}$$

$$C_\alpha := (1-m_\alpha)(K_{1\alpha} - K_{2\alpha}) \tag{41}$$

with $\alpha = f$ or g, and

$$p^a := \frac{1}{3}\boldsymbol{\sigma}\cdot\boldsymbol{\delta}^a, \quad q^a := \sqrt{\frac{3}{2}}\,\|\boldsymbol{s}^a\|, \quad \sin(3\theta^a) = \frac{27}{2}\left(\frac{t^d}{q^d}\right)^3 \tag{42}$$

in which

$$\boldsymbol{s}^a := \boldsymbol{\sigma} - p^a \boldsymbol{\delta}^a, \quad \boldsymbol{d}^a := \mathrm{dev}(\boldsymbol{s}^a), \tag{43}$$

$$\left(q^d\right)^2 := \frac{3}{2}\left\|\boldsymbol{d}^a\right\|, \quad \left(t^d\right)^3 := \frac{1}{3}\,\mathrm{tr}\left(\boldsymbol{d}^{a3}\right). \tag{44}$$

The two functions $M_\alpha(\theta^a, \boldsymbol{\delta}^a)$ appearing in Equations (37) and (38) are provided by the expressions proposed by van Eekelen [38]:

$$M_\alpha(\theta^a, \boldsymbol{\delta}^a) = M_c^\alpha(\theta^a, \boldsymbol{\delta}^a)\, r_M^\alpha(\theta^a) \tag{45}$$

with

$$r_M^\alpha(\theta^a) = k_{1M}^\alpha \left\{1 + k_{2M}^\alpha \sin(3\theta^a)\right\}^{n_\alpha}, \tag{46}$$

$$k_{1M}^\alpha := \frac{1}{2^{n_\alpha}}[1 + (c_M^\alpha)^{1/n_\alpha}]^{n_\alpha}, \quad k_{2M}^\alpha := \frac{1 - (c_M^\alpha)^{1/n_\alpha}}{1 + (c_M^\alpha)^{1/n_\alpha}}, \tag{47}$$

again with $\alpha = f$ or g. The eight quantities a_α, m_α, c_M^α and n_α appearing in (39)–(41), (45) and (46) are material constants, while $\tilde{p}_s$ is a dummy parameter. The nature of the two functions $M_c^\alpha(\theta^a, \boldsymbol{\delta}^a)$ will become clear when the hardening law for $\boldsymbol{\delta}^a$ is discussed in Section 4.1.4.

The typical shape of the yield function described by (35) is shown in Figure 5, in the q-p plane (at $\theta = \pi/6$). The set of internal variables includes the scalar quantity p_s, defining the size of the elastic domain, and the second-order tensor $\boldsymbol{\delta}^a$, which controls its orientation in stress space and accounts for plastic strain-induced anisotropy. Since $\boldsymbol{\delta}^a$ is a director, its norm $\|\boldsymbol{\delta}^a\| = \text{const.} = \sqrt{3}$. The scalars p^a, q^a and θ^a are joint invariants of the second-order tensors $\boldsymbol{\sigma}$ and $\boldsymbol{\delta}^a$, and are similar to those adopted in [39]. The plastic potential and the yield function share the same shape but in general are not coincident. The special case of associative flow ($f \equiv g$) can be obtained by an appropriate choice of the relevant parameters.

4.1.4. *Hardening laws*

The evolution of the scalar internal variable p_s, which plays the same role as the pre-consolidation pressure of classical isotropic-hardening critical-state models (see, *e.g.* [40]), is associated with the first two invariants of the plastic strain rate, as suggested in [41]:

$$\dot{p}_s = \rho_s p_s \left(\dot{\epsilon}_v^{\mathrm{p}} + \xi_s \dot{\epsilon}_s^{\mathrm{p}}\right) = \dot{\lambda}\, \rho_s p_s \left(\hat{T} + \xi_s \hat{N}\right) \tag{48}$$

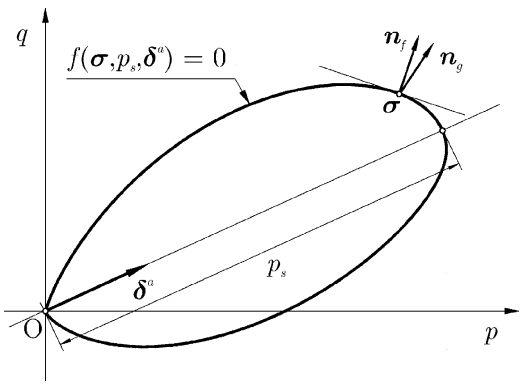

Figure 5. Yield surface of the anisotropic hardening model in the q-p plane.

in which

$$\hat{T} := \mathrm{tr}\left(\boldsymbol{n}_g\right), \quad \hat{N} := \sqrt{\frac{2}{3}}\left\|\mathrm{dev}\left(\boldsymbol{n}_g\right)\right\| \tag{49}$$

and ρ_s and ξ_s are material constants, controlling the rate of expansion/contraction of the yield surface and the balance between deviatoric and volumetric hardening, respectively.

As $\|\boldsymbol{\delta}^a\| = \text{const.}$, the two tensors $\dot{\boldsymbol{\delta}}^a$ and $\boldsymbol{\delta}^a$ must be orthogonal:

$$\dot{\boldsymbol{\delta}}^a \cdot \boldsymbol{\delta}^a = 0.$$

Therefore, the evolution equation for $\boldsymbol{\delta}^a$ is necessarily of the form:

$$\dot{\boldsymbol{\delta}}^a = \dot{\lambda}\, k(\boldsymbol{\sigma}, p_s, \boldsymbol{\delta}^a)\left\{\hat{\boldsymbol{\chi}} - \frac{1}{3}\left(\hat{\boldsymbol{\chi}} \cdot \boldsymbol{\delta}^a\right)\boldsymbol{\delta}^a\right\}, \tag{50}$$

where $\hat{\boldsymbol{\chi}}$ is an arbitrary symmetric second-order tensor. The evolution law (48) inspires the adoption of the following expression for the scalar coefficient k:

$$k(\boldsymbol{\sigma}, \boldsymbol{\delta}^a) = \rho_\delta\left(\hat{T} + \xi_\delta \hat{N}\right), \tag{51}$$

where ρ_δ and ξ_δ are material constants controlling the rate of rotation of the yield surface. Note that, since $\boldsymbol{n}_g$ is independent of p_s, k is a function of $\boldsymbol{\sigma}$ and $\boldsymbol{\delta}^a$ only. Following di Prisco [30,31], the tensor $\hat{\boldsymbol{\chi}}$ is assumed to depend only on the current stress state, according to

$$\hat{\boldsymbol{\chi}} = \cos\hat{\varphi}\,\mathbf{1} + \sqrt{3}\sin\hat{\varphi}\,\frac{\boldsymbol{d}^a}{\left\|\boldsymbol{d}^a\right\|}, \tag{52}$$

where

$$\hat{\varphi}(\theta^a) = \hat{\varphi}_c\, r_\varphi(\theta^a) \tag{53}$$

and

$$r_\varphi(\theta^a) = k_{1\varphi}\left\{1 + k_{2\varphi}\sin(3\theta^a)\right\}^{n_\varphi}, \tag{54}$$

$$k_{1\varphi} := \frac{1}{2^{n_\varphi}}[1 + (c_\varphi)^{1/n_\varphi}]^{n_\varphi}, \quad k_{2\varphi} := \frac{1 - (c_\varphi)^{1/n_\varphi}}{1 + (c_\varphi)^{1/n_\varphi}}. \tag{55}$$

It is easy to recognize from (50) that the tensor $\hat{\boldsymbol{\chi}}$, with $\|\hat{\boldsymbol{\chi}}\| = \sqrt{3}$, is the asymptotic value of $\boldsymbol{\delta}^a$ in the limit condition

$$\left(\dot{\boldsymbol{\sigma}}, \dot{p}_s, \dot{\boldsymbol{\delta}}^a\right) \to (\mathbf{0}, 0, \mathbf{0}).$$

The scalar quantity $\hat{\varphi}$ represents the maximum inclination of the tensor $\hat{\boldsymbol{\chi}}$ with respect to the isotropic axis, and is assumed to depend on the Lode angle via the van Eekelen expression (53), characterized by the three scalar parameters $\hat{\varphi}_c$, c_φ and n_φ. The scalar constant $\hat{\varphi}_c$ is the value of the inclination $\hat{\varphi}$ in axisymmetric compression ($\theta^a = \pi/6$), while the constant c_φ defines the ratio between the values of $\hat{\varphi}$ in axisymmetric extension ($\theta^a = -\pi/6$) and compression.

Anandarajah and Dafalias [39] and di Prisco [30,31] observed that, to better reproduce the available experimental data, the shape of the yield function must change as it rotates. Therefore they included an additional hardening variable to account for shape-hardening effects. In

this work, the simpler strategy is adopted of linking the values of the functions M_c^f and M_c^g appearing in (45) to a scalar measure of the yield surface rotation. In particular, we set

$$M_c^\alpha(\theta^a, \boldsymbol{\delta}^a) = M_{c0}^\alpha + \left(M_{c1}^\alpha - M_{c0}^\alpha\right) \frac{\varphi}{\hat{\varphi}(\theta^a)} \qquad (\alpha = f, g), \tag{56}$$

where the angle φ is defined as

$$\varphi := \cos^{-1}\left(\frac{1}{3}\,\mathrm{tr}\,\boldsymbol{\delta}^a\right). \tag{57}$$

Equation (56) defines a linear interpolation for M_c^α between the two values M_{c0}^α (at $\varphi = 0$) and M_{c1}^α (at $\varphi = \hat{\varphi}$).

4.2. Bounding-Surface model with radial mapping

An important limitation of classical elastoplasticity as applied to geomaterials is represented by the assumption of a large elastic domain, inside which the response of the material is purely reversible. In view of the concepts introduced in Section 2, classical – perfect or hardening – elastoplasticity is characterized by an incrementally bilinear constitutive equation *only* for states on the yield surface. All elastic states are, by definition, endowed with an incrementally linear response. However, a large body of experimental evidence suggests that soil behavior can be irreversible and path-dependent, even for strongly preloaded states, and that plastic yielding is a rather gradual process. Although such effects can be considered of secondary importance in the simulation of monotonic loading paths, it must be noted that a strong dependence of the small-strain stiffness on the loading-path direction has been observed, *e.g.*, by [42,43] in heavily overconsolidated soils, and that such a feature of soil behavior is of great importance in all practical applications in which strong variations of the stress-path direction are expected in different zones of the soil mass, *e.g.*, in the analysis of excavations. Moreover, irreversible (plastic) strains occurring well inside the locus of admissible stress states are obviously of great importance in cyclic loading processes, and the accurate description of such phenomena as cyclic mobility or liquefaction under repeated loading (see, *e.g.* [44]) requires to take these into proper account.

A number of alternative strategies have been proposed to overcome these limitations of the classical theory of plasticity; see for example the review article by [12]. In this work, we consider the two approaches of *Bounding Surface Plasticity* with radial mapping, after Dafalias and coworkers [39,45–47], and *Generalized Plasticity* after Pastor *et al.* [48]. In this section, the former approach is adopted to develop a Bounding Surface version of the basic model described in Section 4.1, while its extension to Generalized Plasticity is detailed in Section 4.3.

The key concept in the formulation of a Bounding Surface model is the fact that the domain $\mathbb{E}_\sigma$ defined by (18) represents the locus of admissible states, rather than the elastic domain of the material. The Bounding Surface (BS), which separates admissible from impossible states, is given by the equation $f(\boldsymbol{\sigma}, \boldsymbol{q}) = 0$, exactly as a standard yield surface in classical plasticity. However, such a surface is *not* a yield surface, as plastic strains can occur for stress states located in its interior.

For stress states lying on the BS, the evolution equations for stress and internal variables are identical to those of the elastoplastic reference model, *viz*. (27)–(29). For states inside the BS, the flow rule $(19)_1$ is modified as follows:

$$\dot{\boldsymbol{\epsilon}}^{\mathrm{p}} = \dot{\lambda}\,\bar{\boldsymbol{n}}_g, \tag{58}$$

in which $\bar{\boldsymbol{n}}_g$ is the plastic flow direction and $\dot{\lambda} \geq 0$ is the plastic multiplier, given by

$$\dot{\lambda} = \frac{1}{\widetilde{K}_p} \left\langle \bar{\boldsymbol{n}}_f \cdot \boldsymbol{D}^{\mathrm{e}} \dot{\boldsymbol{\epsilon}} \right\rangle, \tag{59}$$

where

$$\widetilde{K}_p := \bar{\boldsymbol{n}}_f \cdot \boldsymbol{D}^{\mathrm{e}} \bar{\boldsymbol{n}}_g + \widetilde{H}_p, \tag{60}$$

in which $\bar{\boldsymbol{n}}_f$ is the loading direction, and $\widetilde{H}_p$, by analogy with the standard formulation, plays the role of the plastic modulus.

The definition of $\bar{\boldsymbol{n}}_g$, $\bar{\boldsymbol{n}}_f$ and $\widetilde{H}_p$ requires that, for each stress state $\boldsymbol{\sigma}$ inside the BS a corresponding *image state* $\overline{\boldsymbol{\sigma}}$ is defined on the BS, through a non-invertible *mapping rule*. The mapping rule adopted in this study is a radial mapping with projection center located at the origin of the stress space, as in [45]; see Figure 6. The image state is then given by:

$$\overline{\boldsymbol{\sigma}} = b\,\boldsymbol{\sigma}, \quad b \in [1, \infty). \tag{61}$$

The loading direction, $\bar{\boldsymbol{n}}_f$, and the plastic flow direction, $\bar{\boldsymbol{n}}_g$, are taken as the normalized gradients of the functions f and g at the image state $\overline{\boldsymbol{\sigma}}$:

$$\bar{\boldsymbol{n}}_f := \frac{1}{\bar{f}^*} \frac{\partial f}{\partial \overline{\boldsymbol{\sigma}}}, \quad \bar{\boldsymbol{n}}_g := \frac{1}{\bar{g}^*} \frac{\partial g}{\partial \overline{\boldsymbol{\sigma}}}, \tag{62}$$

while the plastic modulus $\widetilde{H}_p$ is assumed to be a monotonically decreasing function of the distance

$$d := \|\overline{\boldsymbol{\sigma}} - \boldsymbol{\sigma}\| = (b-1)\,\|\boldsymbol{\sigma}\| \tag{63}$$

between the current state and the image state and of the plastic modulus H_p evaluated at $\overline{\boldsymbol{\sigma}}$:

$$\widetilde{H}_p = \widetilde{H}\left(H_p, d\right), \quad \frac{\partial \widetilde{H}}{\partial d} > 0, \quad \widetilde{H}\left(H_p, 0\right) = H_p. \tag{64}$$

After [45] the following expression for the plastic modulus is adopted,

$$\widetilde{H}_p = H_p + \frac{h_{0L} \rho_s p_s}{\bar{f}^* \bar{g}^*} \frac{1}{\langle b/(b-1) - s_L \rangle}, \tag{65}$$

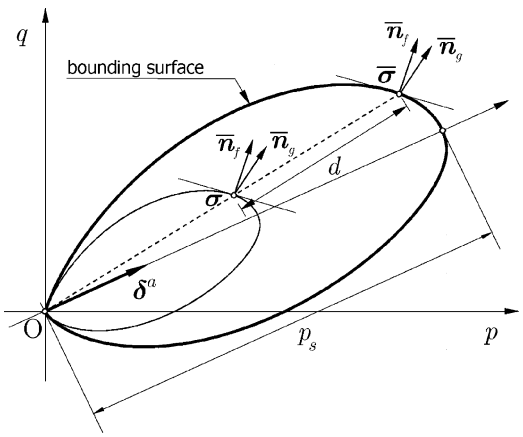

Figure 6. Bounding Surface and radial mapping rule.

in which h_{0L} and $s_L \geq 1$ are two additional material constants. The former controls the stiffness of the material for states far from the BS, while the latter is used to define a region, close to the projection center, known as elastic nucleus. In fact, when b is large enough for the term $[b/(b-1)-s_L]$ to be negative or zero, the plastic modulus in (65) goes to infinity, and the plastic strain rate vanishes. When s_L is close to 1, the elastic nucleus is small (vanishing for $s_L = 1$), whereas it tends to coincide with the BS as $s_L \to \infty$.

4.3. Generalized Plasticity model

A further step towards the extension of classical plasticity to deal with complex loading conditions, taking into account such phenomena as progressive yielding at small strain levels, history-dependence and hysteretic behavior, liquefaction, cyclic mobility or densification, is provided by the framework of *Generalized Plasticity*, first suggested by Zienkiewicz and Mroz [49] and subsequently developed by Pastor *et al.* [48] for applications to cyclic behavior of fine- and coarse-grained soils.

The main feature of Generalized Plasticity is that no plastic potential, yield surface or bounding surface need to be explicitly defined, and no consistency condition is enforced. In Generalized Plasticity the elastic constitutive equation – (15) or (16) – remains the same, whereas the flow rule $(19)_1$ is now replaced by the following evolution laws:

$$\dot{\boldsymbol{\epsilon}}^{\mathrm{p}} = \dot{\lambda}_L \boldsymbol{n}_{gL} \quad \text{if} \quad \boldsymbol{n}_L \cdot \boldsymbol{D}^{\mathrm{e}} \dot{\boldsymbol{\epsilon}} \geq 0, \tag{66}$$

$$\dot{\boldsymbol{\epsilon}}^{\mathrm{p}} = \dot{\lambda}_U \boldsymbol{n}_{gU} \quad \text{if} \quad \boldsymbol{n}_L \cdot \boldsymbol{D}^{\mathrm{e}} \dot{\boldsymbol{\epsilon}} < 0, \tag{67}$$

in which the plastic multipliers for loading ($\dot{\lambda}_L$) and unloading ($\dot{\lambda}_U$) are given by

$$\dot{\lambda}_L = \frac{1}{\widehat{K}_{pL}} \boldsymbol{n}_L \cdot \boldsymbol{D}^{\mathrm{e}} \dot{\boldsymbol{\epsilon}}, \quad \dot{\lambda}_U = \frac{1}{\widehat{K}_{pU}} \boldsymbol{n}_L \cdot \boldsymbol{D}^{\mathrm{e}} \dot{\boldsymbol{\epsilon}} \tag{68}$$

with

$$\widehat{K}_{pL} := \boldsymbol{n}_L \cdot \boldsymbol{D}^{\mathrm{e}} \boldsymbol{n}_{gL} + \widehat{H}_{pL}, \tag{69}$$

$$\widehat{K}_{pU} := \boldsymbol{n}_L \cdot \boldsymbol{D}^{\mathrm{e}} \boldsymbol{n}_{gU} + \widehat{H}_{pU}. \tag{70}$$

In Equation (66)–(70), $\boldsymbol{n}_L$, $\boldsymbol{n}_{gL}$ and $\boldsymbol{n}_{gU}$ define the loading direction, the plastic-flow direction for plastic loading and the plastic-flow direction for plastic unloading (*reverse loading*), respectively, while the scalars $\widehat{H}_{pL}$ and $\widehat{H}_{pU}$ are the corresponding plastic moduli for (plastic) loading and unloading. All these quantities are considered as prescribed functions of the state variables $(\boldsymbol{\sigma}, \boldsymbol{q})$, to be determined from the main features of the observed behavior of the material, but not necessarily deriving from any yield function, plastic potential, or consistency condition.

In order to develop a Generalized Plasticity model which could be thought of as a hierarchical extension of the elastoplastic model presented in Section 4.1 and of the corresponding Bounding Surface version of Section 4.2, the choice is made here to assume

$$\boldsymbol{n}_L \equiv \bar{\boldsymbol{n}}_f, \quad \boldsymbol{n}_{gL} \equiv \bar{\boldsymbol{n}}_g, \tag{71}$$

with $\bar{\boldsymbol{n}}_f$ and $\bar{\boldsymbol{n}}_g$ given by (62). This amounts to identifying the loading tensor with the unit normal to the bounding surface $f(\boldsymbol{\sigma}, p_{\mathrm{s}}, \boldsymbol{\delta}^{\alpha}) = 0$ at the image state $\bar{\boldsymbol{\sigma}}$ – given by (61) – and the plastic-flow direction in loading with the normalized gradient of the plastic potential at $\bar{\boldsymbol{\sigma}}$ (see Figure 7). As for the plastic-flow direction in unloading, guided by the results

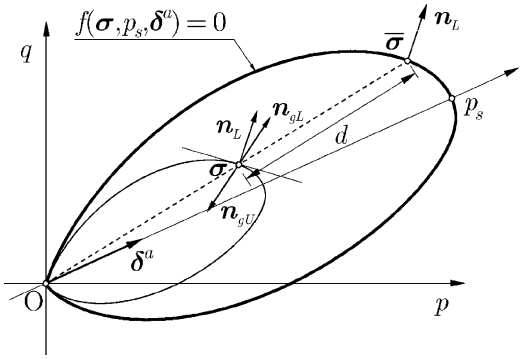

Figure 7. Definition of loading tensor $\boldsymbol{n}_L$ and plastic flow directions for loading, $\boldsymbol{n}_{gL}$, and unloading, $\boldsymbol{n}_{gU}$.

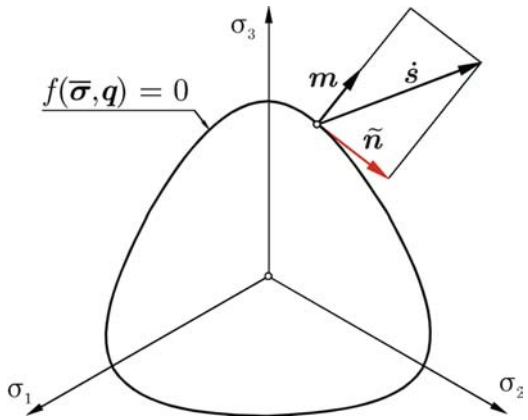

Figure 8. Geometrical interpretation of tensors $\boldsymbol{m}$ and $\tilde{\boldsymbol{n}}$ in the deviatoric plane.

obtained in DEM simulations of deviatoric probing tests, see [20], the simple choice of setting $\boldsymbol{n}_{gU}=-\boldsymbol{n}_{gL}$ has been adopted.

For states on the bounding surface, the plastic modulus $\widehat{H}_{pL}$ is given by $(25)_2$, as in the classical elastoplastic model, while $\widehat{H}_{pU}\to\infty$. For states inside the bounding surface, both plastic moduli are continuous functions of $H_p(\overline{\boldsymbol{\sigma}})$ and of the distance d between the current state and the image state:

$$\widehat{H}_{pL}=H_p+\frac{h_{0L}\rho_s p_s}{\overline{f}^*\overline{g}^*}\,\frac{1}{\langle b/(b-1)-s_L\rangle}, \tag{72}$$

$$\widehat{H}_{pU}=H_p+\frac{h_{0U}\rho_s p_s}{\overline{f}^*\overline{g}^*}\,\frac{1}{\langle b-s_U\rangle^{\beta}}, \tag{73}$$

where h_{0L}, $s_L\geq 1$, h_{0U}, $s_U\geq 1$ and β are material constants. Equation (72) is identical to (65). The simple expression adopted for the plastic modulus in unloading, $\widehat{H}_{pU}$, provides very high values close to the bounding surface ($b=\infty$ for $b\leq s_U$), which decrease with increasing distance between the current state and the image state.

4.4. Generalized tangential plasticity

The third and last extension of the basic elastoplastic model presented in Section 4.1 has been obtained by equipping the Generalized Plasticity model of Section 4.3 with the concept of a *tangential* flow rule, as proposed by Papamichos and Vardoulakis [50]. This choice is motivated by the DEM results presented in [20], which indicate that the direction of plastic-strain increments in the deviatoric plane may not be unique, and depends, in general, on the stress-increment direction.

According to [50], the additive strain decomposition in Equation (14) must be modified as follows:

$$\dot{\boldsymbol{\epsilon}}=\dot{\boldsymbol{\epsilon}}^{\mathrm{e}}+\dot{\boldsymbol{\epsilon}}^{\mathrm{p}}_{\parallel}+\dot{\boldsymbol{\epsilon}}^{\mathrm{p}}_{\perp}. \tag{74}$$

In the above equation, $\dot{\boldsymbol{\epsilon}}^{\mathrm{p}}_{\parallel}$ represents the conventional plastic-strain rate, given by the flow rule (66) – loading – or (67) – unloading – while $\dot{\boldsymbol{\epsilon}}^{\mathrm{p}}_{\perp}$ is an additional contribution to the plastic strain rate, known as *tangential* plastic strain rate.

The term tangential used for $\dot{\boldsymbol{\epsilon}}^{\mathrm{p}}_{\perp}$ refers to its direction with respect to the unit normal $\boldsymbol{n}_{\mathrm{L}}$ to the bounding surface. In fact, the amount of tangential plastic strain rate is governed by the following flow rule:

$$\dot{\boldsymbol{\epsilon}}^{\mathrm{p}}_{\perp} = \frac{1}{h_1}\widetilde{\boldsymbol{n}}, \tag{75}$$

where

$$\widetilde{\boldsymbol{n}} := \boldsymbol{I}_{\perp}\dot{\boldsymbol{s}}, \quad \boldsymbol{I}_{\perp} := \boldsymbol{I} - \boldsymbol{m}\otimes\boldsymbol{m}, \quad \boldsymbol{m} := \frac{\operatorname{dev}\left(\boldsymbol{D}^{\mathrm{e}}\boldsymbol{n}_L\right)}{\left\|\operatorname{dev}\left(\boldsymbol{D}^{\mathrm{e}}\boldsymbol{n}_L\right)\right\|} \tag{76}$$

and h_1 is a material constant, known as tangential plastic modulus. In the particular case of isotropic elasticity, $\boldsymbol{m}$ is normal to the bounding surface in the deviatoric plane, and $\widetilde{\boldsymbol{n}}$ represents the projection of the deviatoric stress rate, $\dot{\boldsymbol{s}}$, onto the tangent plane to the bounding surface at the image point (see Figure 8).

The particular choice of $\widetilde{\boldsymbol{n}}$ allows to retain the expressions given by (68) for the plastic multipliers $\dot{\lambda}_L$ and $\dot{\lambda}_U$. In fact, for states on the bounding surface, the consistency condition upon plastic loading reads

$$\dot{f} = f^{*}\boldsymbol{n}_L\cdot\boldsymbol{D}^{\mathrm{e}}\left[\dot{\boldsymbol{\epsilon}} - \dot{\lambda}_L\boldsymbol{n}_{gL} - \frac{1}{h_1}\widetilde{\boldsymbol{n}}\right] + \dot{\lambda}_L\frac{\partial f}{\partial \boldsymbol{q}}\cdot\boldsymbol{h} = 0$$

which yields

$$\begin{aligned}\dot{\lambda}_L &= \frac{1}{\boldsymbol{n}_L\cdot\boldsymbol{D}^{\mathrm{e}}\boldsymbol{n}_{gL} + H_p}\left(\boldsymbol{n}_L\cdot\boldsymbol{D}^{\mathrm{e}}\dot{\boldsymbol{\epsilon}} - \frac{1}{h_1}\boldsymbol{n}_L\cdot\boldsymbol{D}^{\mathrm{e}}\widetilde{\boldsymbol{n}}\right)\\ &= \frac{1}{\boldsymbol{n}_L\cdot\boldsymbol{D}^{\mathrm{e}}\boldsymbol{n}_{gL} + H_{\mathrm{p}}}\boldsymbol{n}_L\cdot\boldsymbol{D}^{\mathrm{e}}\dot{\boldsymbol{\epsilon}},\end{aligned} \tag{77}$$

since, according to (76), $\boldsymbol{n}_L\cdot\boldsymbol{D}^{\mathrm{e}}\widetilde{\boldsymbol{n}} = \widetilde{\boldsymbol{n}}\cdot\boldsymbol{D}^{\mathrm{e}}\boldsymbol{n}_L = 0$. The above result motivates the adoption of the same expressions (68), even for states inside the bounding surface, with the plastic moduli now given by (72) and (73).

Combining the elastic constitutive equation in rate form with the flow rules for the two components of the plastic-strain rate, we have:

$$\dot{\boldsymbol{\sigma}} = \boldsymbol{D}^{ep}\dot{\boldsymbol{\epsilon}} - \boldsymbol{D}^{\mathrm{e}}\dot{\boldsymbol{\epsilon}}^{\mathrm{p}}_{\perp}, \tag{78}$$

where

$$\boldsymbol{D}^{ep} := \boldsymbol{D}^{\mathrm{e}} - \frac{1}{\widehat{K}_{pL/\mathrm{U}}}\left(\mathbf{D}^{\mathrm{e}}\mathbf{n}_{gL/U}\right)\otimes\left(\boldsymbol{n}_L\boldsymbol{D}^{\mathrm{e}}\right) \tag{79}$$

is the elastoplastic tangent stiffness tensor, with plastic moduli and plastic-flow directions properly selected for loading or unloading according to the strain-rate direction.

The tangential plastic-strain rate appearing in the last term on the RHS of (78) can be expressed as a function of the total strain rate as follows. Let

$$\boldsymbol{I}_{\mathrm{dev}} := \boldsymbol{I} - \frac{1}{3}\mathbf{1}\otimes\mathbf{1}, \quad \boldsymbol{N} := \boldsymbol{I}_{\perp}\boldsymbol{I}_{\mathrm{dev}} = \boldsymbol{I} - \boldsymbol{m}\otimes\boldsymbol{m} - \frac{1}{3}\mathbf{1}\otimes\mathbf{1}. \tag{80}$$

Then, according to Equations (75), (72), (73) and (79), we have:

$$\dot{\boldsymbol{\epsilon}}_{\perp}^{\mathrm{p}} = \frac{1}{h_1}\boldsymbol{N}\dot{\boldsymbol{\sigma}} = \frac{1}{h_1}\boldsymbol{N}\boldsymbol{D}^{\mathrm{e}}\left(\dot{\boldsymbol{\epsilon}} - \dot{\lambda}_{L/U}\boldsymbol{n}_{gL/U} - \dot{\boldsymbol{\epsilon}}_{\perp}^{\mathrm{p}}\right)$$
$$= \frac{1}{h_1}\boldsymbol{N}\boldsymbol{D}^{ep}\dot{\boldsymbol{\epsilon}} - \frac{1}{h_1}\boldsymbol{N}\boldsymbol{D}^{\mathrm{e}}\dot{\boldsymbol{\epsilon}}_{\perp}^{\mathrm{p}}. \tag{81}$$

Solving for $\dot{\boldsymbol{\epsilon}}_{\perp}^{\mathrm{p}}$, we obtain

$$\dot{\boldsymbol{\epsilon}}_{\perp}^{\mathrm{p}} = \boldsymbol{K}^{-1}\boldsymbol{N}\boldsymbol{D}^{ep}\dot{\boldsymbol{\epsilon}} \tag{82}$$

in which

$$\boldsymbol{K} := h_1\boldsymbol{I} + \boldsymbol{N}\boldsymbol{D}^{\mathrm{e}}. \tag{83}$$

Finally, substituting (83) in (78), we obtain the constitutive equation in rate form as:

$$\dot{\boldsymbol{\sigma}} = \left\{\boldsymbol{D}^{\mathrm{ep}} - \boldsymbol{D}^{\mathrm{e}}(\boldsymbol{K}^{-1}\boldsymbol{N})\boldsymbol{D}^{\mathrm{ep}}\right\}\dot{\boldsymbol{\epsilon}}. \tag{84}$$

It is worth noting that the constitutive equation of the Generalized Plasticity model is recovered from (84) as $h_1 \to \infty$.

5. Predicted *vs.* experimental responses

In the following, the DEM response obtained from the stress-probing programs discussed in Section 3.3 is compared to the predictions of the three extended plasticity models discussed in Section 4. Herein, the comparison is intended mainly as a tool to evaluate the *qualitative* features of the directional response of the different constitutive equations. Accordingly, no detailed calibration of the relevant material parameters has been performed for the three models. Rather, the different sets of material parameters adopted in the simulations (reported in Table 2) have been assigned taking as a starting point the results of a single DEM simulation of an axisymmetric, drained compression test, as reported in [9]. Some quantitative differences between model predictions and DEM responses are therefore to be expected.

5.1. Axisymmetric probes

5.1.1. *Virgin initial state B*

The discrete DEM response to axisymmetric stress probes (Figure 2a) with $\|\Delta\boldsymbol{\sigma}\| = 10\,\mathrm{kPa}$, starting from the (virgin) initial state B, is shown in Figure 9. The corresponding predictions of the bounding surface model (BS), generalized plasticity model (GP) and generalized tangential plasticity model (GTP) are shown in Figures 10 and 11, respectively. Note that for this particular loading condition, the response of the GP and GTP models are identical, as $\widetilde{\boldsymbol{n}} = \boldsymbol{0}$.

As has already been observed in our previous publications, see *e.g.* [20], the overall behavior of the DEM model at the virgin state B conforms to that of a classical elastoplastic model with a single plastic mechanism. In particular, Figure 9 shows that the total and elastic response envelopes are nearly coincident within a significant portion of the Rendulic plane of strain increments, and that the plastic RE nearly collapses into a single line, which indicates that the plastic flow direction does not depend on the imposed loading direction.

The envelopes predicted by the BS model (Figure 10) reproduce quite well this pattern of response. A good agreement is also observed between DEM simulations and the predictions of the two Generalized Plasticity models (Figure 11), with the only possible exception of a slight overestimation of plastic-strain increments in unloading conditions, which are not

Table 2. Material parameters adopted for BS, GP and GTP models.

Model	α (–)	$\hat{\kappa}$ (–)	G_0 (MPa)	p_r (kPa)	a_f (–)	m_f (–)	c_M^f (–)	M_{c0}^f (–)	M_{c1}^f (–)
BS	0·0	0·0037	24·1	100·0	0·7	0·9999	0·9	0·7	0·6
GP	0·0	0·0037	24·1	100·0	0·7	0·9999	0·9	0·7	0·6
GTP	0·0	0·0037	24·1	100·0	0·7	0·9999	0·9	0·7	0·6
Model	a_g (–)	m_g (–)	c_M^g (–)	M_{c0}^g (–)	M_{c1}^g (–)	ρ_s (–)	ξ_s (–)	ρ_δ (–)	ξ_δ (–)
BS	0·8	0·9999	0·9	1·2	1·08	250·0	0·47	100·0	0·2
GP	0·8	0·9999	0·9	1·2	1·08	250·0	0·47	100·0	0·2
GTP	0·8	0·9999	0·9	1·2	1·08	250·0	0·47	100·0	0·2
Model		$\hat{\phi}_c$ (–)	h_{0L} (–)	s_L (–)	h_{0U} (–)	s_U (–)	β (–)	h_1 (MPa)	
BS		0·2	1·0	1·005	—	—	—	—	
GP		0·2	1·0	1·005	1·5	1·005	1·5	—	
GTP		0·2	1·0	1·005	1·5	1·005	1·5	200·0	

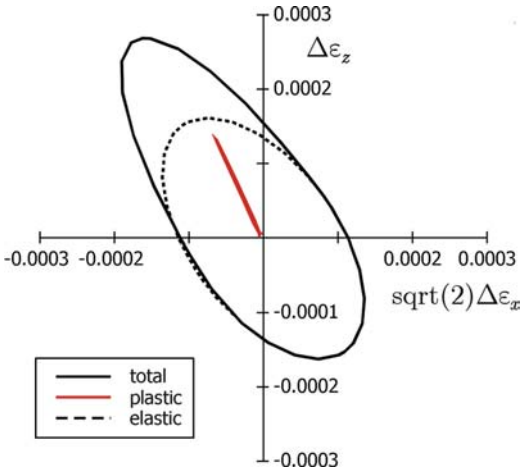

Figure 9. Axisymmetric response envelopes for virgin initial state B: DEM results.

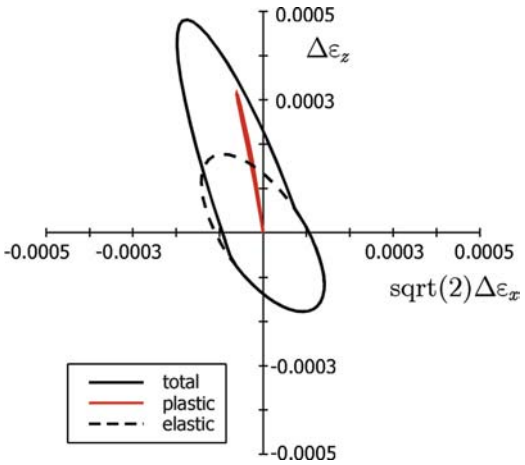

Figure 10. Axisymmetric response envelopes for virgin initial state B: BS model predictions.

detectable in the DEM results. Actually, the DEM behavior at this particular initial state could be equally well reproduced by the classical elastoplastic model outlined in Section 4.1.

5.1.2. *Preloaded initial state B′*

The most striking feature of the incremental response exhibited by the DEM model upon axisymmetric stress probing starting from the preloaded state B′, see Figure 12, is that plastic strains do occur for almost all the prescribed loading directions. These plastic-strain increments are definitely lower in magnitude as compared to those observed at the corresponding virgin state B. In a first approximation, they could be neglected if the main interest is in the

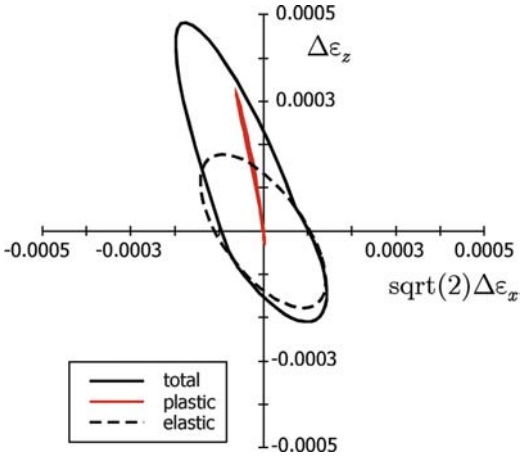

Figure 11. Axisymmetric response envelopes for virgin initial state B: GP and GTP model predictions.

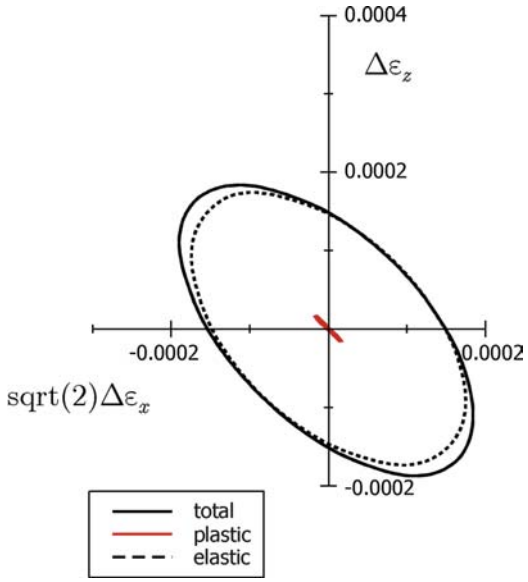

Figure 12. Axisymmetric response envelopes for preloaded initial state B′: DEM results.

modeling of gross yield phenomena at medium to large strain levels. In this case, the use of classical plasticity would be appropriate. If, however, the focus is on the constitutive modeling of material behavior at small strains, then the data clearly show the need for a more general constitutive framework. More specifically, the DEM response at the preloaded state indicates:

(i) the lack of a discernible elastic range, as plastic loading occurs for all the stress probes except for two 'neutral loading' directions, symmetric about the origin;
(ii) the existence of two distinct plastic-flow directions which, for all practical purposes, can be assumed to be coincident, but with opposite orientation.

While the BS model can predict reasonably well the pattern of plastic strains for those stress probes which induce plastic loading conditions, its response to stress probes in the opposite directions remains elastic; see Figure 13. On the contrary, the response of the GP and GTP models, shown in Figure 14, reproduces quite well these features. Although some discrepancies exist and are noticeable in the plastic-flow direction, these are solely due to details of the model formulations and/or inaccurate characterization of the relevant material parameters.

Overall, the GP and GTP models – due to their ability of developing plastic deformations in unloading – are capable of correctly reproducing the observed pattern of irreversible behavior. In particular, the fact that in generalized plasticity the plastic loading/unloading conditions are controlled by a single loading direction is consistent with feature (i), whereas it is the observation (ii) which motivated our choice about the plastic-flow direction in unloading.

5.2. Deviatoric probes

Figure 15 shows the discrete DEM responses for deviatoric stress probes with $\|\Delta\boldsymbol{\sigma}\| = 10\,\text{kPa}$ (see Figure 2b). Only the virgin state B is considered hereafter. As observed in [20], a clear dependence of the direction of plastic-strain increments on the stress-probe direction is apparent. In the deviatoric plane, the plastic RE does not collapse into a single line, but rather is a closed loop, symmetric about the $\Delta\epsilon_z$ axis. Note that the direction of the plastic-strain increments in the Rendulic plane, not shown here, is almost constant and coincident

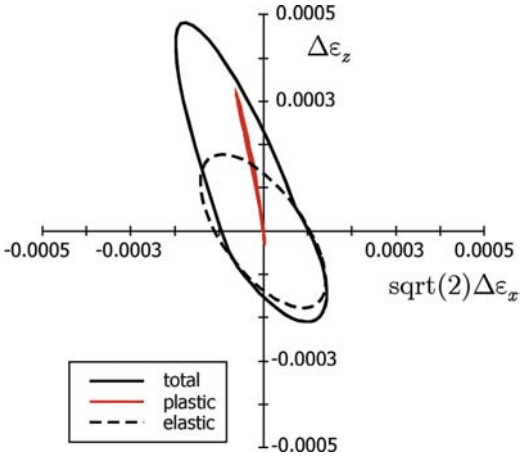

Figure 13. Axisymmetric response envelopes for pre-loaded initial state B′: BS model predictions.

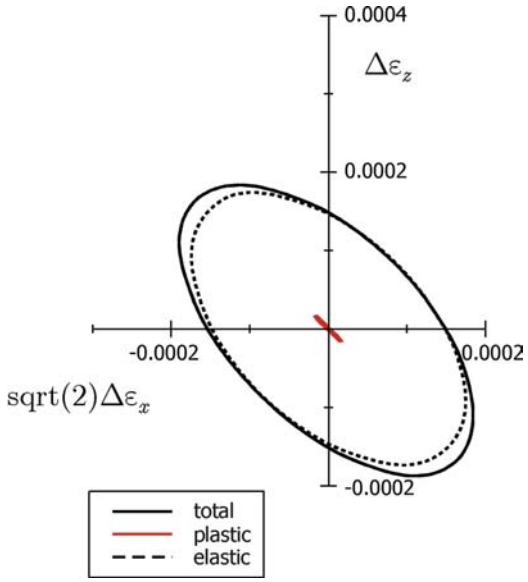

Figure 14. Axisymmetric response envelopes for pre-loaded initial state B′: GP and GTP model predictions.

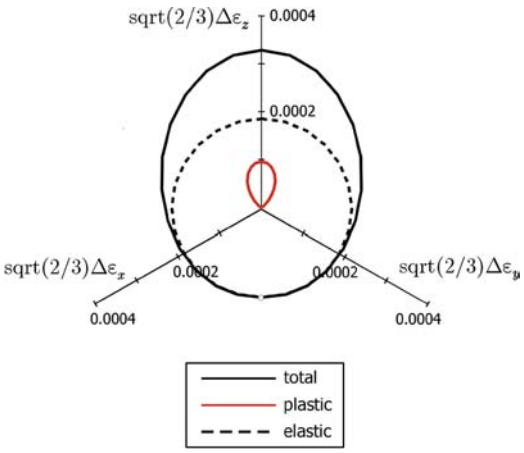

Figure 15. Deviatoric response envelopes for virgin initial state B: DEM results.

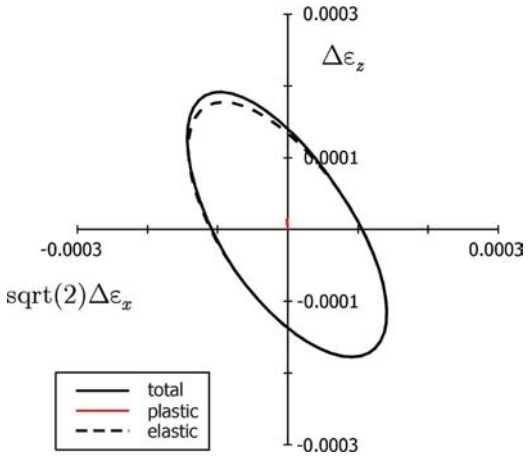

Figure 16. Deviatoric response envelopes for virgin initial state B: BS model predictions.

with the direction of incremental plastic-strains as computed in the axisymmetric case (Figure 9). Results also indicate that the plastic-strain increments corresponding to stress probes orthogonal to the $\Delta\sigma_z$ axis are not negligible.

The response of the BS model is shown in Figure 16. For infinitesimal stress probes, the plastic RE should be a single line parallel to the $\Delta\epsilon_z$ axis. However, this is not the case here, as the envelope does show some dependence of plastic-strain increments on the applied stress increment direction, although this effect is small, *i.e.*, the plastic RE is rather flat about the $\Delta\epsilon_z$ axis. It is worth noting that this particular feature of the plastic-response envelope is not to be attributed to any incremental nonlinearity of the constitutive equation, but is rather a consequence of the finite size of the stress increment and of the high curvature of the plastic potential at the initial stress state. For probes which deviate from the $\Delta\sigma_z$ axis, the current state is no longer axisymmetric as soon as the stress

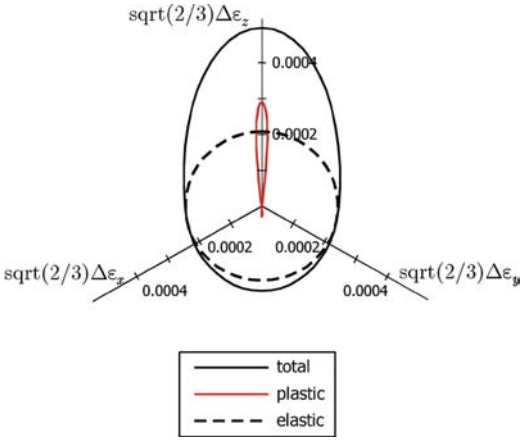

Figure 17. Deviatoric response envelopes for virgin initial state B: GP model predictions.

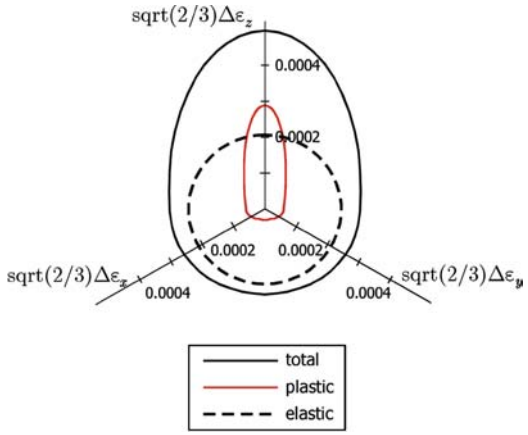

Figure 18. Deviatoric response envelopes for virgin initial state B: GTP model predictions.

increment brings the state of the material out of the so-called triaxial plane. In such conditions, the plastic strain rate changes continuously direction in the deviatoric plane, following the curvature of the plastic-potential function.

The response of the GP model, shown in Figure 17, is quite close to that of the BS model, except for the appearance of some small plastic-strain increments in unloading, which are not detected in the DEM simulations. The assumption of a single loading mechanism, controlled by tensor $\boldsymbol{n}$, is reflected in the existence of two 'neutral loading' directions, orthogonal to the $\Delta\sigma_z$ axis, according to the symmetry of the initial stress state and specimen microstructural features (induced anisotropy). This is however in sharp contrast with the observed DEM behavior (see Figure 15), as in the DEM simulations total and elastic-strain increments appear to be nearly coincident in a region of the strain-increment space which is approximately bounded by the traces of the $\Delta\epsilon_x$ and $\Delta\epsilon_y$ axes, forming an angle of about $2\pi/3$.

Such a deficiency of the GP model, which is shared by all plasticity theories with a single loading mechanism, was the main motivation for the introduction of tangential plasticity in the GP formulation. This has the effect of allowing plastic deformation for all the possible loading directions, as shown in Figure 18. The plastic RE, resulting from the sum of the normal and tangential contributions (see Figure 19), has now a lower aspect ratio, as compared to the plastic RE of the GP model. In particular, as the tangential component of the plastic strain attains its maximum for the two loading directions which are orthogonal to the axisymmetric stress plane (*i.e.*, for the two neutral loading directions of the GP model), the plastic envelope is rather large along the horizontal direction in the deviatoric plane of strain increments. However, such a feature of the plastic RE is not apparent in the plastic RE obtained in the DEM simulations, and therefore, the introduction of tangential plasticity in conventional or extended elastoplastic formulations as a mean to provide the constitutive equations with a certain degree of incremental non linearity does not appear completely satisfactory – from both a quantitative and a qualitative point of view.

6. Concluding remarks

The emphasis of this paper has been on the evaluation of extended plasticity theories for modeling the qualitative features of material response, as observed for an analogue granular material, as a function of the previous stress history and loading conditions. A key assump-

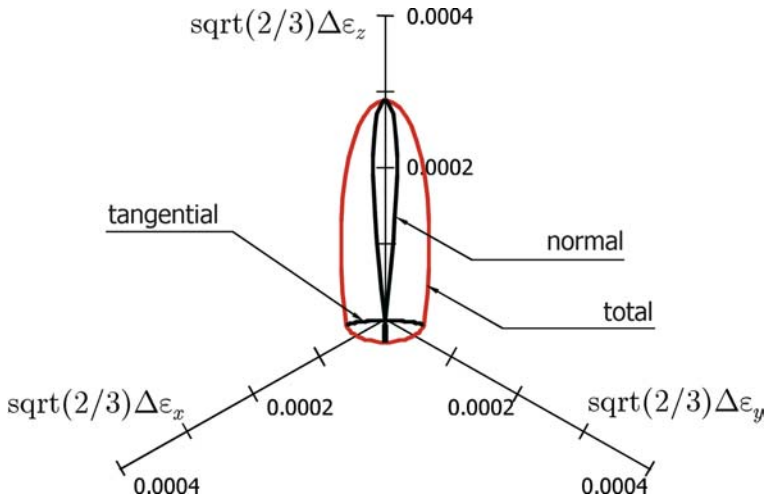

Figure 19. Deviatoric probing at virgin initial state B: detail of plastic response envelope of GTP model.

tion of the present work is that the adopted DEM model sand is capable of displaying all the relevant features of the incremental behavior of real granular soils. In fact, this has been confirmed in a number of previous studies; see *e.g.* [9,21].

The main results obtained in this investigation can be summarized as follows:

1. The observed behavior of the model sand upon stress-probing in the deviatoric plane, starting from a virgin, axisymmetric stress state, departs from the basic assumptions of classical plasticity, as the direction of the plastic strain vector in the strain increment space does depend on the stress-probe direction.
2. The observed behavior of the model sand upon axisymmetric probing from a preloaded state also departs from the basic assumptions of classical plasticity, as non-negligible plastic-strain increments are observed, even inside the so-called 'state boundary surface', separating admissible from impossible stress states in stress space.
3. Upon axisymmetric probing from a preloaded state, plastic strains do occur for (almost) all probing directions. This is clear evidence of the occurrence of reverse plastic loading, which cannot be properly described by such generalizations of classical plasticity as radial mapping Bounding Surface models.
4. Generalized Plasticity appears more suitable than Bounding Surface plasticity for capturing reverse-loading effects observed in axisymmetric probing tests.
5. Tangential Plasticity is effective in introducing a certain degree of dependence of plastic strain increment direction on loading direction (*i.e.*, incremental nonlinearity). However, the qualitative response obtained does not appear to be completely satisfactory. Whether more general approaches to incremental nonlinearity, such as, for example, the theory of hypoplasticity [51,52], can perform better in this respect, is still an open question.

References

1. V.V. Sokolowski, *Statics of Granular Media*. Oxford: Pergamon (1965) 270 pp.
2. W.F. Chen, *Limit Analysis and Soil Plasticity*. Amsterdam: Elsevier (1976) 637 pp.
3. K.H. Roscoe and J.B. Burland, On the generalised stress–strain behaviour of 'wet' clay. In: J. Heyman and F.A. Leckie (eds.), *Engineering Plasticity*. Cambridge: Cambridge Univ. Press (1968) pp. 535–609.
4. A.N. Schofield and C.P. Wroth, *Critical State Soil Mechanics*. London: McGraw-Hill (1968) 310 pp.

5. G. Gudehus, F. Darve and I. Vardoulakis (eds.), *Constitutive Relations for Soils*. Rotterdam: Balkema (1984) 497 pp.
6. A.S. Saada and G.F. Bianchini (eds.), *Constitutive Equations for Granular Non-Cohesive Soils*. Rotterdam: Balkema (1989) 733 pp.
7. D. Kolymbas (ed.), *Modern Approaches to Plasticity*. Amsterdam: Elsevier (1993) 780 pp.
8. D. Kolymbas (ed.), *Constitutive Modelling of Granular Materials*. Berlin: Springer (1999) 554 pp.
9. F. Calvetti, G. Viggiani and C. Tamagnini, A numerical investigation of the incremental behavior of granular soils. *Rivista Italiana di Geotecnica*, 37 (2003) 11–29.
10. C.A. Truesdell and W. Noll, The non-linear field theories of mechanics. In: S. Flügge (ed.), *Encyclopedia of Physics*, vol. III/3. Berlin: Springer (1965) pp. 1–602
11. D.R. Owen and W.O. Williams, On the time derivatives of equilibrated response functions. *Arch. Rat'l. Mech. Anal.* 33 (1969) 288–306.
12. C. Tamagnini and G. Viggiani, Constitutive modelling for rate-independent soils: a review. *Revue Française de Génie Civil.* 6 (2002) 933–974.
13. F. Darve, The expression of rheological laws in incremental form and the main classes of constitutive equations. In: F. Darve (ed.), *Geomaterials: Constitutive Equations and Modelling*. Amsterdam: Elsevier (1990) pp. 123–148.
14. A. Anandarajah, K. Sobhan and N. Kuganenthira, Incremental stress–strain behavior of a granular soil. *J. Geotech. Engng. ASCE* 121 (1995) 57–68.
15. P. Royis and T. Doanh, Theoretical analysis of strain response envelopes using incrementally non-linear constitutive equations. *Int. J. Num. Anal. Meth. Geomech.* 22 (1998) 97–132.
16. J.-P. Bardet and J. Proubet, Application of micromechanics to incrementally nonlinear constitutive equations for granular media. In: J. Biarez and R. Gourves (eds.), *Proc. Powders and Grains 1989*. Rotterdam: Balkema (1989) pp. 265–273.
17. J.-P. Bardet, Numerical tests with discrete element method. In: D. Kolymbas (ed.), *Proc. Modern Approaches to Plasticity*. Amsterdam: Elsevier (1993) pp. 179–197.
18. J.-P. Bardet, Numerical simulations of the incremental responses of idealized granular materials. *Int. J. Plasticity* 10 (1994) 879–908.
19. F. Calvetti and C. di Prisco, Fabric evolution of granular materials: a numerical approach. In: *Proc. First Forum Young European Researchers*. Liege, Belgium (1993) pp. 115–120.
20. F. Calvetti, C. Tamagnini and G. Viggiani, On the incremental behaviour of granular soils. In G.N. Pande and S. Pietruszczak (eds.), *Proc. NUMOG VIII*. Rotterdam: Balkema (2002) pp. 3–10.
21. F. Calvetti, G. Viggiani and C. Tamagnini, Micromechanical inspection of constitutive modelling. In: C. Viggiani (ed.), *Constitutive Modelling and Analysis of Boundary Value Problems in Geotechnical Engineering*. Benevento: Hevelius (2003) pp. 187–216.
22. ITASCA. *PFC–3D User Manual*, Itasca Consulting Group, Minneapolis (1995) 110 pp.
23. P.A. Cundall, A computer model for simulating progressive large scale movements in blocky rock systems. In: *Proc. Symp. ISRM*, Nancy, France. Rotterdam: Balkema (1971) Paper no. II–8.
24. P.A. Cundall and O.D.L. Strack, A discrete numerical model for granular assemblies. *Géotechnique* 29 (1979) 47–65.
25. P.A. Cundall and R.D. Hart, Numerical modeling of discontinua. *Engg. Comp*. 9 (1992) 101–113.
26. Y. Kishino and C. Thornton, Discrete element approaches. In: F. Oka and T. Tamura (eds.), *Mechanics of Granular Materials. An Introduction*. Rotterdam: Balkema (1999) pp. 147–223.
27. C. Tamagnini, G. Viggiani, R. Chambon and J. Desrues, Evaluation of different strategies for the integration of hypoplastic constitutive equations: Application to the cloe model. *Mech. Cohesive–Frictional Mater* 5 (2000) 263–289.
28. G. Gudehus, A comparison of some constitutive laws for soils under radially symmetric loading and unloading. In: Wittke (ed.), *3rd Int. Conf. Num. Meth. Geomech.* Rotterdam: Balkema (1979) pp. 1309–1324.
29. R. Nova, Sinfonietta classica: an exercise on classical soil modelling. In: Saada and Bianchini (eds.), *Constitutive Equations for Granular Non-Cohesive Soils*. Rotterdam: Balkema (1988) pp. 501–519.
30. C. di Prisco, *Sand Anisotropy: Experimental Analysis and Mathematical Modelling.* PhD thesis, Politecnico di Milano (1993) 222 pp. (in Italian).
31. C. di Prisco, R. Nova and J.Lanier, A mixed isotropic–kinematic hardening constitutive law for sand. In: D. Kolymbas (ed.), *Modern Approaches to Plasticity*. Amsterdam: Elsevier (1993) pp. 83–124.
32. R. Nova and D.M. Wood, A constitutive model for sand in triaxial compression. *Int. J. Num. Anal. Meth. Geomech.* 3 (1979) 255–278.

33. C. Tamagnini, R. Castellanza and R. Nova, A generalized backward euler algorithm for the numerical integration of an isotropic hardening elastoplastic model for mechanical and chemical degradation of bonded geomaterials. *Int. J. Num. Anal. Meth. Geomech.* 26 (2002) 963–1004.
34. J.C. Simo and T.J.R. Hughes, *Computational Inelasticity*. Berlin: Springer (1997) 392 pp.
35. G. Maier, On associative incremental elastic-plastic constitutive models. *Rend. Ist. Lombardo di Scienze e Lettere* 100 (1966) 809–838. (in Italian).
36. R.I. Borja and C. Tamagnini, Cam–clay plasticity, part III: Extension of the infinitesimal model to include finite strains. *Comp. Meth. Appl. Mech. Engng*. 155 (1998) 73–95.
37. R. Lagioia, A.M. Puzrin and D.M. Potts, A new versatile expression for yield and plastic potential surfaces. *Comput. Geotech.* 19 (1996) 171–191.
38. H.A.M. van Eekelen, Isotropic yield surfaces in three dimensions for use in soil mechanics. *Int. J. Numer. Anal. Meth. Geomech.* 4 (1980) 89–101.
39. A. Anandarajah and Y.F. Dafalias, Bounding surface plasticity. III: Application to anisotropic cohesive soils. *J. Engng. Mech., ASCE* 112 (1986) 1292–1318.
40. D.M. Wood, *Soil Behaviour and Critical State Soil Mechanics*. Cambridge: Cambridge Univ. Press (1990) 462 pp.
41. R. Nova, On the hardening of soils. *Arch. Mech. Stosowanej* 29 (1977) 445–458.
42. J.H. Atkinson, D. Richardson and S.E. Stallebrass, Effect of recent stress history on the stiffness of overconsolidated clay. *Géotechnique* 40 (1986) 531–540.
43. S.E. Stallebrass, *Modelling the Effect of Recent Stress History on the Behaviour of Overconsolidated Soils*. PhD thesis. The City University, London (1990) 164 pp.
44. D.M. Wood, Laboratory investigations of the behaviour of soils under cyclic loading: a review. In: G.N. Pande and O.C. Zienkiewicz (eds.), *Soil Mechanics – Cyclic and Transient Loads*. Chichester: Wiley (1982) pp. 513–582.
45. Y.F. Dafalias and L.R. Herrmann, Bounding surface formulation of soil plasticity. In: G.N. Pande and O.C. Zienkiewicz (eds.), *Soil Mechanics – Cyclic and Transient Loads*. Chichester: Wiley (1982) pp. 253–283.
46. Y.F. Dafalias, Bounding surface plasticity. I: Mathematical foundation and hypoplasticity. *J. Engng. Mech., ASCE* 112 (1986) 966–987.
47. Y.F. Dafalias and L. R. Herrmann, Bounding surface plasticity. II: Application to isotropic cohesive soils. *J. Engng. Mech., ASCE* 112 (1986) 1263–1291.
48. M. Pastor, O.C. Zienkiewicz and A.H.C. Chan, Generalized plasticity and the modelling of soil behaviour. *Int. J. Numer. Anal. Meth. Geomech.* 14 (1990) 151–190.
49. O.C. Zienkiewicz and Z. Mroz, Generalized plasticity formulation and applications to geomechanics. In: C.S. Desai and R.H. Gallagher (eds.), *Mechanics of Engineering Materials*. Chichester: Wiley (1984) pp. 655–679.
50. E. Papamichos and I. Vardoulakis, Shear band formation in sand according to non–coaxial plasticity model. *Géotechnique* 4 (1995) 649–661.
51. D. Kolymbas, An outline of hypoplasticity. *Arch. Appl. Mech.* 61 (1991) 143–151.
52. C. Tamagnini, G. Viggiani and R. Chambon, A review of two different approaches to hypoplasticity. In: D. Kolymbas (ed.), *Constitutive Modelling of Granular Materials*. Berlin: Springer (2000) pp. 107–145.